# Chapter 2
# Object of Research

This chapter describes the objects of research i.e. a two-wheeled mobile robot and a robotic manipulator with three degrees of freedom. It presents the structure, components and basic parameters of the controlled systems. The chapter discusses the kinematics of both robots and provides a simulation for solving the inverse kinematics problem. The desired trajectory of a given system was generated, based on a pre-planned path and velocity values of a selected point attached to a robot. The generated trajectories were used for numerical tests and verification analyses of tracking performance with regard to the controlled systems. The chapter discusses also the dynamics of both controlled systems and provides a simulation for solving the inverse dynamics problem for a given trajectory generated earlier. This resulted in waveforms of control signals for a given trajectory.

## 2.1 Two-Wheeled Mobile Robot

Pioneer 2-DX wheeled mobile robot (WMR) is a two-wheeled robot intended for laboratory use. It is equipped with the so-called caster, which is a third self-adjusting supporting wheel, whose dynamics was not taken into consideration, and is assumed to be negligible. Mobile robots with a similar structure are known as two-wheeled robots since they have two drive wheels. It is to be noted that in the last few years new robots have been introduced that have no extra supporting wheel.

The Pioneer 2-DX model [1] is shown in Fig. 2.1a, while its dimensional representation is shown in Fig. 2.1b.

The model is composed of:

- drive wheels 1 and 2,
- caster 3,
- frame 4.

© Springer International Publishing AG 2018

M. Szuster and Z. Hendzel, *Intelligent Optimal Adaptive Control for Mechatronic Systems*, Studies in Systems, Decision and Control 120,
https://doi.org/10.1007/978-3-319-68826-8_2

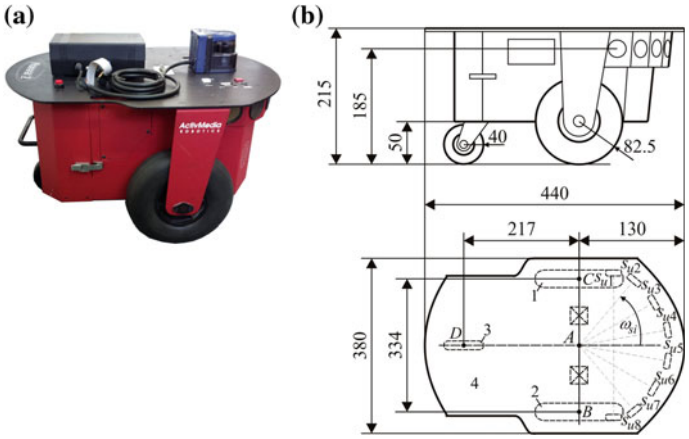



**Fig. 2.1** **a** Pioneer 2-DX wheeled mobile robot. **b** Pioneer 2-DX schematic diagram; main physical dimensions

Pioneer 2's total mass is $m_{DX} = 9$ [kg], and its maximum capacity (payload) is $m_{Lx} = 20$ [kg]. Drive wheels 1 and 2 are made of rubber and their main physical dimensions are: radius $r = r_1 = r_2 = 0.0825$ [m] and width $h_{w1} = h_{w2} = 0.037$ [m].

The maximum velocity of point $A$, which is attached to the Pioneer 2-DX WMR, is $v_{mx} = 1.6$ [m/s]. The WMR is equipped with a sensory system consisting of 8 ultrasonic sensors, affixed to the circumference on the front of the frame. The sensors are denoted by $s_{u1}, \ldots, s_{u8}$ as marked in Fig. 2.1b. In the programming phase, the maximum measuring range of rangefinders was limited to $d_{mx} = 4$ [m]. If the distance between an obstacle and the WMR is greater than the adopted limit, a default value $d_{mx}$ is assumed. The minimum measuring distance from an obstacle is $d_{mn} = 0.4$ [m]. If the distance between an obstacle and the WMR is less than $d_{mn}$, a default value $d_{mn}$ is assumed. Considering the above, the distance measurements made by the ultrasonic sensors fall in the range $d_{si} \in \langle 0.4, 4.0 \rangle$[m], $i = 1, \ldots, 8$. The deviations of ultrasonic sensors' axes from the frame's axis of symmetry are as follows: $\omega_{s1} = 90°$, $\omega_{s2} = 50°$, $\omega_{s3} = 30°$, $\omega_{s4} = 10°$, $\omega_{s5} = -10°$, $\omega_{s6} = -30°$, $\omega_{s7} = -50°$, $\omega_{s8} = -90°$.

An analysis of the WMRs motion is linked to the kinematics and dynamics of these objects which is further discussed in the subchapters below.

### *2.1.1 Description of the Kinematics of a Mobile Robot*

The issues related to the kinematics of the WMR include, inter alia, forward and inverse kinematics problems. A problem-solving approach to forward kinematics consists in the determination of the WMR's position and orientation relative to a stationary frame of reference, where the motion parameters of the drive units and

the geometry of the system are known. To solve the inverse kinematics problem, the angular parameters of drive wheels rotation need to be determined, given that a predefined path and velocity of a selected point of the system are known. An analysis of the inverse kinematics problem is carried out to determine the trajectory of the WMR that is to be executed by the tracking control system [7, 21].

Selection of a characteristic WMR's point that is to follow the desired path depends on the vehicle's navigation system and the design of the control system. The desired path for a selected WMR's point is represented by rectilinear and curvilinear segments [19] so as to ensure the completion of a defined task. There are many factors that affect the path design such as the type of tasks to be carried out, the structure and technical capabilities of the WMR. Section 7.8 provides a synthesis of the WMR's trajectory generation layer of the hierarchical control system. The layer generates control signals that are necessary to determine the trajectory for the WMR's selected point. This process is carried out on an ongoing basis during the performance of tasks such as "goal seeking with obstacle avoidance", which is a combination of two task types: "goal seeking"and "keep to the center of the empty space/obstacle avoidance".

The kinematics of a selected point of the system is analyzed by means of kinematic equations that may be established through application of different methods e.g. Denavit–Hartenberg convention [19] which employs homogenous coordinates and transformation matrices. Another approach is to use the classic methods applied in mechanics, in particular an analytical description of motion that is based on the parametric equations of motion [21].

In the following considerations it is assumed that all the WMR's components are perfectly rigid and the motion is executed on a flat horizontal surface. The WMR motion is described based on a model (see Fig. 2.2) corresponding to the structure of the Pioneer 2–DX robot used in the verification of solutions that are presented later in this work. The investigated WMR is a nonholonomic system with two degrees

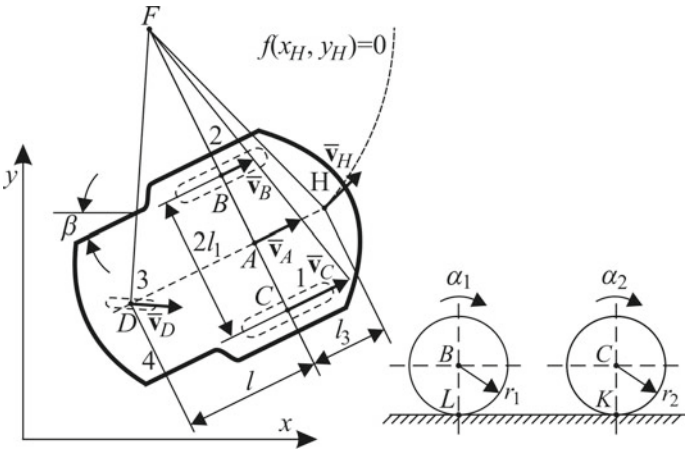



**Fig. 2.2** Schematic diagram of velocities of individual points on wheeled mobile robot's frame

of freedom. Two independent variables were used for motion description i.e. drive wheels 1 and 2 rotation angles, denoted by $\alpha_1$ and $\alpha_2$, respectively. In the case where angular velocity vectors of the WMR drive wheels take the same values, the robot's frame performs translational motion, whereas if angular velocity vectors of individual wheels have different values, the robot's frame is in plane motion (i.e. it moves in the plane (surface) of motion defined by axes $xy$).

In the analysis of the inverse kinematics problem, it was assumed that the selected point $H$ on the WMR moves on a given path with a desired velocity. The execution of trajectory is ensured by defining appropriate angular velocities for the rotation of the WMR drive wheels 1 and 2. It is also assumed that the WMR wheels roll without slipping and the velocity vector of the characteristic point $A$ lies in the plane parallel to the plane of motion and is directed perpendicularly to a line segment bounded by points $B$ and $C$ [7, 21].

In the case where the velocities of points $B$ and $C$ are such that $v_B > v_C$, the WMR's frame is in the plane motion and point $F$ shown in Fig. 2.2 is the instantaneous center of rotation of the frame.

Projections of the WMR's point $A$ velocity vector on stationary coordinate system axes $x$ and $y$ satisfy the relation

$$\dot{y}_A = \dot{x}_A \tan(\beta) \ , \tag{2.1}$$

where $\beta$ – instantaneous angle of rotation of the WMR's frame.

It follows from Eq. (2.1) that point $A$ velocity vector is bounded by nonholonomic constraints. Based on the geometry of the WMR the relation between points $H$ and $A$ in the $xy$ system can be determined

$$x_H = x_A + l_3 \cos(\beta) \ , \tag{2.2}$$

$$y_H = y_A + l_3 \sin(\beta) \ . \tag{2.3}$$

Differentiating the above relations with respect to time, we get

$$\dot{x}_H = \dot{x}_A + l_3 \dot{\beta} \sin(\beta) \ , \tag{2.4}$$

$$\dot{y}_H = \dot{y}_A + l_3 \dot{\beta} \cos(\beta) \ . \tag{2.5}$$

Given that $v_A$ is the value of point $A$ velocity vector, then values of vector projections on the coordinate system axes $xy$ are as follows

$$\dot{x}_A = v_A \cos(\beta) \ , \tag{2.6}$$

$$\dot{y}_A = v_A \sin(\beta) \ . \tag{2.7}$$

Plugging relations (2.6) and (2.7) into the set of Eqs. (2.4) and (2.5), we obtain

$$\dot{x}_H = v_A \cos(\beta) + l_3 \dot{\beta} \sin(\beta) \ , \tag{2.8}$$

$$\dot{y}_H = v_A \sin(\beta) + l_3 \dot{\beta} \cos(\beta) \ . \tag{2.9}$$

It is assumed that point $H$ moves in the $xy$ plane, on a path that is analytically expressed as

$$f(x_H, y_H) = 0 \ , \tag{2.10}$$

where by differentiating (2.10) with respect to time, we get

$$\dot{f}(x_H, y_H) = 0 \ . \tag{2.11}$$

Given the velocity of point $A$ and the desired path of point $H$, the set of Eqs. (2.8), (2.9) and (2.11) allows for the calculation of the change in the values of the following parameters

$$\begin{aligned} x_H &= x_H(t) \ , \\ y_H &= y_H(t) \ , \\ \beta &= \beta(t) \ . \end{aligned} \tag{2.12}$$

Relations that describe the velocities of points $B$ and $C$, when written as vectors, take the following form

$$\begin{aligned} \overline{\mathbf{v}}_C &= \overline{\mathbf{v}}_A + \overline{\mathbf{v}}_{CA} \ , \\ \overline{\mathbf{v}}_B &= \overline{\mathbf{v}}_A + \overline{\mathbf{v}}_{BA} \ , \end{aligned} \tag{2.13}$$

and in the scalar form

$$\begin{aligned} v_C &= v_A + v_{CA} \ , \\ v_B &= v_A + v_{BA} \ , \end{aligned} \tag{2.14}$$

where

$$\begin{aligned} v_{CA} &= \dot{\beta} l_1 \ , \\ v_{BA} &= -\dot{\beta} l_1 \ . \end{aligned} \tag{2.15}$$

It is assumed that the WMR drive wheels roll without slipping, hence the following relations are satisfied

$$\begin{aligned} v_B &= \dot{\alpha}_1 r_1 \ , \\ v_C &= \dot{\alpha}_2 r_2 \ , \end{aligned} \tag{2.16}$$

where $r_1 = r_2 = r$ – radiuses of the WMR drive wheels.

By considering Eqs. (2.14)–(2.16), the angular velocities $\dot{\alpha}_1$ and $\dot{\alpha}_2$ of individual WMR drive wheels can be written as

$$\begin{bmatrix} \dot{\alpha}_1 \\ \dot{\alpha}_2 \end{bmatrix} = \frac{1}{r} \begin{bmatrix} 1 & l_1 \\ 1 & -l_1 \end{bmatrix} \begin{bmatrix} v_A \\ \dot{\beta} \end{bmatrix} \ . \tag{2.17}$$

The inverse form of relation (2.17) takes the form

$$\begin{bmatrix} v_A \\ \dot{\beta} \end{bmatrix} = \frac{r}{2} \begin{bmatrix} 1 & 1 \\ l_1^{-1} & l_1^{-1} \end{bmatrix} \begin{bmatrix} \dot{\alpha}_1 \\ \dot{\alpha}_2 \end{bmatrix} . \tag{2.18}$$

Kinematic relations described by Eqs. (2.17) and (2.18) are considered later in this work. To solve the inverse kinematics problem the values of the following variables need to be calculated

$$\begin{aligned} x_H &= x_H(t) , \\ y_H &= y_H(t) , \\ \beta &= \beta(t) , \\ \dot{\alpha}_1 &= \dot{\alpha}_1(t) , \\ \dot{\alpha}_2 &= \dot{\alpha}_2(t) . \end{aligned} \tag{2.19}$$

by means of Eqs. (2.8), (2.9), (2.11) and (2.19), taking into account the desired path for point $H$ and the velocity of point $A$ $v_A$.

Given that distance $l_3 = 0$, two trajectories of point $A$ were generated relative to the desired paths. The first being a loop-shaped path with loop radius $R = 0.75$ [m], and the second being an 8-shaped path consisting of two combined loops, each of radius $R = 0.75$ [m].

#### 2.1.1.1 Simulation of Loop-Shaped Path Inverse Kinematics

The WMR's point $A$ motion on the desired loop-shaped path, from the initial position at point $S$ to the desired final position at point $G$, is divided into five characteristic phases [7]:

(a) Start-up (motion on a rectilinear path):

$$v_A = \frac{v_A^*}{t_r - t_p}\left(t - t_p\right) , \quad t_p \le t < t_r , \quad \dot{\alpha}_1 = \dot{\alpha}_2 = \frac{v_A}{r} , \quad \dot{\beta} = 0 ,$$

where $v_A$ – linear velocity of point $A$, $t$ – time, $v_A^*$ – maximum desired linear velocity of point $A$, $t_p$ – (motion) initial time, $t_r$ – end-time of start-up, $\dot{\alpha}_1, \dot{\alpha}_2$ – desired angular velocities of the WMR drive wheels rotation, $r$ – drive wheel radius, $\dot{\beta}$ – instantaneous angular velocity of the WMRs frame rotation.

(b) Motion with the desired velocity, when $v_A = v_A^*$ = const.:

$$\dot{\alpha}_1 = \dot{\alpha}_2 = \frac{v_A}{r} , \quad t_r \le t < t_{c1} , \quad \dot{\beta} = 0 ,$$

where $t_{c1}$ – start-time of curvilinear motion.

(c) Motion in a circular path with radius $R$, when $v_A = v_A^* = \text{const.}$, $R = 0.75$ [m]:

$$\dot{\alpha}_1 = \frac{v_A}{r} + l_1\dot{\beta} \ , \quad \dot{\alpha}_2 = \frac{v_A}{r} - l_1\dot{\beta} \ , \quad t_{c1} \le t < t_{c2} \ ,$$

where $t_{c2}$ – end-time of curvilinear motion, $l_1$ – length that results from the WMR's geometry.

(d) Curve exit including the transition period, followed by motion on a rectilinear path with constant velocity, when $v_A = v_A^* = \text{const.}$:

$$\dot{\alpha}_1 = \dot{\alpha}_{p1} - \left(\dot{\alpha}_{p1} - \frac{v_A}{r}\right)\left(1 - e^{-\varsigma t}\right) \ , \ \dot{\alpha}_2 = \dot{\alpha}_{p2} - \left(\frac{v_A}{r} - \dot{\alpha}_{p2}\right)\left(1 - e^{-\varsigma t}\right) \ ,$$
$$t_{c2} \le t < t_h \ ,$$

where $t_h$ – braking start-time, $\varsigma$ – transition curves approximation constant, $\dot{\alpha}_{p1}, \dot{\alpha}_{p2}$ – values of wheels' angular velocities at the beginning of the transition period. Introducing approximation allows for the execution of system's motion with smooth changes being applied to parameters such as velocity and acceleration.

(e) Braking:

$$v_A = v_A^* - \frac{v_A^*}{t_k - t_h}(t - t_h) \ , \quad t_h \le t < t_k \ , \quad \dot{\alpha}_1 = \dot{\alpha}_2 = \frac{v_A}{r} \ , \quad \dot{\beta} = 0 \ ,$$

where $t_k$ – end-time.

Equal lengths of time were adopted for the braking and the start-up phase. The start-time values for the remaining phases are respectively: $t_p = 3$ [s], $t_r = 5$ [s], $t_{c1} = 7.5$ [s], $t_{c2} = 20.5$ [s], $t_h = 23$ [s], $t_k = 25$ [s]. The maximum linear velocity value of point $A$ on the WMR is $v_A^* = 0.4$ [m/s]. To eliminate discontinuities in angular accelerations of trajectory with a triangular velocity profile, an approximation of the velocity profile was generated by means of the following relation

$$v_A = v_A^* \cdot \frac{1}{\left(1 + \exp^{-c_1(t-t_1)}\right)\left(1 + \exp^{c_1(t-t_2)}\right)} \ , \tag{2.20}$$

where $c_1 = 12$ [1/s] – sigmoid functions slope coefficients, $t_1$ – motion mean start-time, $t_1 = 0.5(t_r + t_p) = 4$ [s], $t_2$ – braking mean start-time, $t_2 = 0.5(t_k + t_h) = 24$ [s]. The diagrams of the assumed triangular velocity profile and its approximation are shown in Fig. 2.3a, b, respectively.

Based on the desired velocity profile (Fig. 2.3b), the desired motion path of point $A$ on the WMR (Fig. 2.4a) and the geometry of the WMR, the inverse kinematics problem was solved, thereby producing angular variables related to the WMR drive wheels rotation. Figure 2.4b shows the diagram of rotation angles $\alpha_1$ and $\alpha_2$ [rad] of the WMR drive wheels, Fig. 2.4c presents the angular velocities $\dot{\alpha}_1$ and $\dot{\alpha}_2$ [rad/s], whereas in Fig. 2.4d the angular accelerations $\ddot{\alpha}_1$ and $\ddot{\alpha}_2$ [rad/s$^2$] are presented.

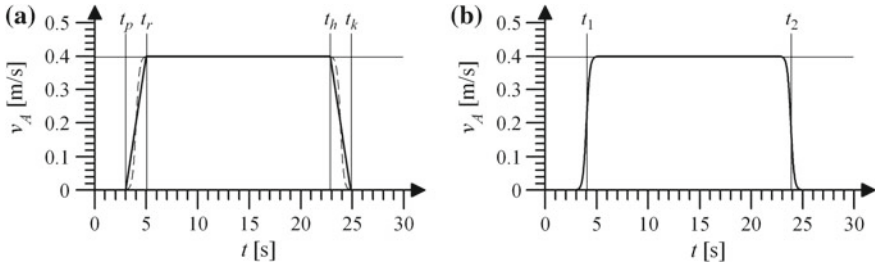



**Fig. 2.3** **a** WMR's point $A$ triangular velocity profile, **b** approximation of point $A$ triangular velocity profile

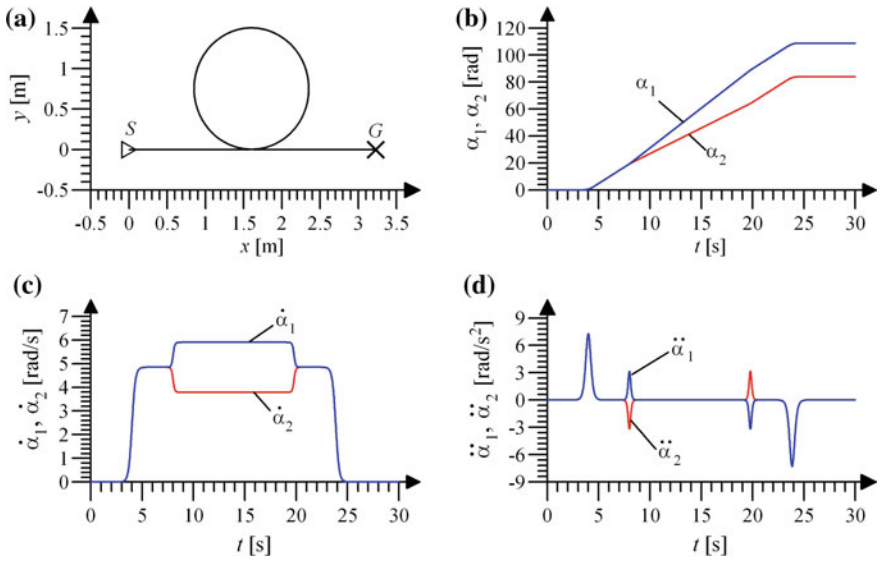



**Fig. 2.4** **a** WMR's point $A$ desired motion path, **b** WMR drive wheels rotation angles $\alpha_1$ and $\alpha_2$, **c** angular velocities $\dot{\alpha}_1$ and $\dot{\alpha}_2$, **d** angular accelerations $\ddot{\alpha}_1$ and $\ddot{\alpha}_2$

### 2.1.1.2 Simulation of 8-Shaped Path Inverse Kinematics

The WMR's point $A$ motion on the desired 8-shaped path, from the initial position at point $S$ to the desired final position at point $G$, is divided into two characteristic phases (I and II), each of which consists in a "drive" on a loop-shaped path. Motion phases are separated by a stop at point $P$. Each phase consists of nine characteristic sub-phases of motion:

(a) Start-up (motion in a rectilinear path):

$$v_A = \frac{v_A^*}{t_{r1} - t_{p1}} \left(t - t_{p1}\right) \ , \quad t_{p1} \le t < t_{r1} \ , \quad \dot{\alpha}_1 = \dot{\alpha}_2 = \frac{v_A}{r} \ , \quad \dot{\beta} = 0 \ ,$$

where $t_{p1}$ – initial time of motion in the first phase of motion, $t_{r1}$ – start-up end-time in the first phase of motion.

(b) Motion with the desired velocity, when $v_A = v_A^* = \text{const.}$:

$$\dot{\alpha}_1 = \dot{\alpha}_2 = \frac{v_A}{r} \ , \quad t_{r1} \leq t < t_{c1} \ , \quad \dot{\beta} = 0 \ ,$$

where $t_{c1}$ – start-time of the curvilinear motion in the first phase of motion.

(c) Motion along a circular path with radius $R$, when $v_A = v_A^* = \text{const.}$, $R = 0.75$ [m]:

$$\dot{\alpha}_1 = \frac{v_A}{r} + l_1\dot{\beta} \ , \quad \dot{\alpha}_2 = \frac{v_A}{r} - l_1\dot{\beta} \ , \quad t_{c1} \leq t < t_{a1} \ ,$$

where $t_{a1}$ – start-time of decrease in velocity (deceleration) in the curvilinear motion.

(d) Deceleration in the motion along a circular path with radius $R$:

$$\dot{\alpha}_1 = \frac{v_A^* - \left(v_A^* - v_A^{**}\right) \cdot (t - t_{a2})}{r\,(t_{a2} - t_{a1})} + l_1\dot{\beta} \ , \quad \dot{\alpha}_2 = \frac{v_A^* - \left(v_A^* - v_A^{**}\right) \cdot (t - t_{a2})}{r\,(t_{a2} - t_{a1})} - l_1\dot{\beta} \ ,$$
$$t_{a1} \leq t < t_{a2} \ ,$$

where $t_{a2}$ – end-time of deceleration in the curvilinear motion, $v_A^{**}$ – minimum desired linear velocity of the selected point $A$ on the WMR.

(e) Motion along a circular path with radius $R$, when $v_A = v_A^{**} = \text{const.}$, $R = 0.75$ [m]:

$$\dot{\alpha}_1 = \frac{v_A}{r} + l_1\dot{\beta} \ , \quad \dot{\alpha}_2 = \frac{v_A}{r} - l_1\dot{\beta} \ , \quad t_{a2} \leq t < t_{a3} \ ,$$

where $t_{a3}$ – start-time of increase in velocity (acceleration) in the curvilinear motion.

(f) Acceleration in the motion on a circular path with radius $R$:

$$\dot{\alpha}_1 = \frac{v_A^* - \left(v_A^* - v_A^{**}\right) \cdot (t_{a3} - t)}{r\,(t_{a3} - t_{a4})} + l_1\dot{\beta} \ , \ \dot{\alpha}_2 = \frac{v_A^* - \left(v_A^* - v_A^{**}\right) \cdot (t_{a3} - t)}{r\,(t_{a3} - t_{a4})} - l_1\dot{\beta} \ ,$$
$$t_{a3} \leq t < t_{a4} \ ,$$

where $t_{a4}$ – end-time of acceleration in the curvilinear motion.

(g) Motion on a circular path with radius $R$, when $v_A = v_A^* = \text{const.}$, $R = 0.75$ [m]:

$$\dot{\alpha}_1 = \frac{v_A}{r} + l_1\dot{\beta} \ , \quad \dot{\alpha}_2 = \frac{v_A}{r} - l_1\dot{\beta} \ , \quad t_{a4} \leq t < t_{c2} \ .$$

where $t_{c2}$ – end-time of the curvilinear motion in the first phase of motion.

(h) Curve exit including the transition period, followed by motion on a rectilinear path with constant velocity, when $v_A = v_A^* = \text{const.}$:

$$\dot{\alpha}_1 = \dot{\alpha}_{p1} - \left(\dot{\alpha}_{p1} - \frac{v_A}{r}\right)\left(1 - e^{-\varsigma t}\right) \ , \ \dot{\alpha}_2 = \dot{\alpha}_{p2} - \left(\frac{v_A}{r} - \dot{\alpha}_{p2}\right)\left(1 - e^{-\varsigma t}\right) \ ,$$
$$t_{c2} \leq t < t_{h1} \ ,$$

where $t_{h1}$ – braking start-time in the first phase of motion, $\varsigma$ – transition curves approximation constant, $\dot{\alpha}_{p1}, \dot{\alpha}_{p2}$ – values of wheels' angular velocities at the beginning of the transition period in the first phase of motion.

(i) Braking:

$$v_A = v_A^* - \frac{v_A^*}{t_{k1} - t_{h1}} (t - t_{h1}) \ , \quad t_{h1} \leq t < t_{k1} \ , \quad \dot{\alpha}_1 = \dot{\alpha}_2 = \frac{v_A}{r} \ , \quad \dot{\beta} = 0 \ .$$

The second characteristic period of the WMR's point $A$ motion on a loop-shaped path consists of identical motion phases.

Equal lengths of time were adopted for the braking and the start-up phase, equal lengths of time were assumed for the decrease and increase in velocities in the curvilinear motion phase. The start-time values for the subsequent phases are respectively: $t_{p1} = 3$ [s], $t_{r1} = 5$ [s], $t_{c1} = 7.5$ [s], $t_{a1} = 10$ [s], $t_{a2} = 11$ [s], $t_{a3} = 13.85$ [s], $t_{a4} = 14.85$ [s], $t_{c2} = 18$ [s], $t_{h1} = 18.4$ [s], $t_{k1} = 20.4$ [s], $t_{p2} = 24.6$ [s], $t_{r1} = 26.6$ [s], $t_{c3} = 22.2$ [s], $t_{b1} = 30.1$ [s], $t_{b2} = 31.1$ [s], $t_{b3} = 34.1$ [s], $t_{b4} = 35.1$ [s], $t_{c4} = 32.8$ [s], $t_{h2} = 40$ [s], $t_{k2} = 42$ [s]. The maximum velocity value of point $A$ on the WMR is $v_A^* = 0.4$ [m/s], whereas the minimum is $v_A^{**} = 0.3$ [m/s]. To eliminate the discontinuities in angular accelerations of trajectory with a triangular velocity profile, an approximation of the velocity profile was generated by means of the following relation

$$v_A = v_A^* \cdot \sum_{m=0}^{1} \frac{1}{\left(1 + exp^{-c_1(t - t_{1+4m})}\right)\left(1 + exp^{c_1(t - t_{4+4m})}\right)} + \\ - \left(v_A^* - v_A^{**}\right) \cdot \sum_{m=0}^{1} \frac{1}{\left(1 + exp^{-c_2(t - t_{2+4m})}\right)\left(1 + exp^{c_2(t - t_{3+4m})}\right)} \ , \qquad (2.21)$$

where $c_1 = 6$ [1/s], $c_2 = 12$ [1/s] – sigmoid functions slope coefficients, $t_1$ – start-up's mean start-time in the first phase of motion, $t_1 = 0.5\left(t_{r1} + t_{p1}\right) = 4$ [s], $t_2$ – mean start-time of deceleration in the curvilinear motion in the first phase of motion, $t_2 = 0.5\left(t_{a1} + t_{a2}\right) = 10.5$ [s], $t_3$ – mean start-time of acceleration in the curvilinear motion, $t_3 = 0.5\left(t_{a3} + t_{a4}\right) = 14.35$ [s], $t_4$ – braking mean start-time, $t_4 = 0.5\left(t_{k1} + t_{h1}\right) = 19.4$ [s], $t_5$ – start-up's mean start-time in the second phase of motion, $t_5 = 0.5\left(t_{r2} + t_{p2}\right) = 25.6$ [s], $t_6$ – mean start-time of deceleration in the curvilinear motion in the second phase of motion, $t_6 = 0.5\left(t_{b1} + t_{b2}\right) = 30.6$ [s], $t_7$ – mean start-time of acceleration in the curvilinear motion, $t_7 = 0.5\left(t_{b3} + t_{b4}\right) = 33.6$ [s], $t_8$ – braking mean start-time, $t_8 = 0.5\left(t_{k2} + t_{h2}\right) = 41$ [s]. The diagrams of the assumed triangular velocity profile and its approximation are shown in Fig. 2.5a, b, respectively.

Based on the desired velocity profile (Fig. 2.5b), the desired motion path of point $A$ on WMR (Fig. 2.6a) and the geometry of the Pioneer 2-DX, the inverse kinematics problem was solved, thereby producing angular variables of the WMR drive wheels rotation. Figure 2.6b shows the diagram of rotation angles $\alpha_1$ and $\alpha_2$ [rad] of the WMR

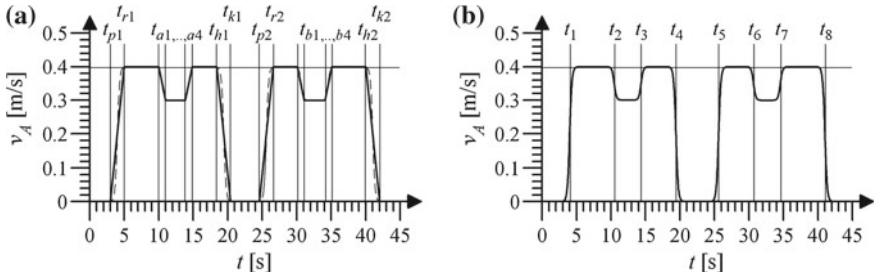



**Fig. 2.5** **a** WMR point *A* triangular velocity profile, **b** approximation of point *A* triangular velocity profile

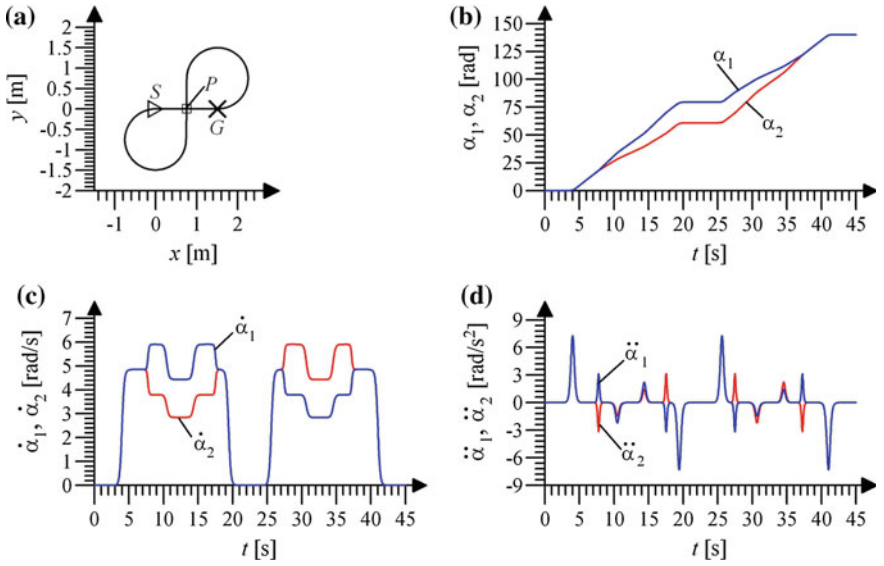



**Fig. 2.6** **a** WMR point *A* desired motion path, **b** WMR drive wheels rotation angles $\alpha_1$ and $\alpha_2$, **c** angular velocities $\dot{\alpha}_1$ and $\dot{\alpha}_2$, **b** angular accelerations $\ddot{\alpha}_1$ and $\ddot{\alpha}_2$

drive wheels, Fig. 2.6c presents the angular velocities $\dot{\alpha}_1$ and $\dot{\alpha}_2$ [rad/s], whereas in Fig. 2.6d the angular accelerations $\ddot{\alpha}_1$ and $\ddot{\alpha}_2$ [rad/s$^2$] are presented.

The generated solutions to the inverse kinematics problem were applied in the quality analysis of tracking performance with regard to particular control systems, as the WMR's desired trajectory.

### *2.1.2 Description of the Dynamics of a Mobile Robot*

The analysis of issues related to the WMR's dynamics consists in seeking correlations between the system's parameters of motion and the mechanisms that cause the

motion. The forward dynamics problem is to determine the system's parameters of motion resulting from the generalized forces, whose values are known, whereas the inverse dynamics problem is solved by determining the values of the generalized forces that occur during the WMR's motion along the desired trajectory, where the values of the parameters of motion are known [21].

The analysis of the WMR's dynamics results in a mathematical model represented by ordinary differential equations that may be used for further analysis, identification of parameters and synthesis of control systems [11]. The model that describes the WMR's dynamics provides merely an approximation of real system's behavior and does not take into account every system-related event, due to the computational complexity and difficulty in measuring certain quantities.

The WMRs are complex mechanical systems with nonholonomic constraints and a nonlinear dynamic description. The dynamics of such systems can be described by means of Lagrange equations with multipliers [7, 21] to obtain dynamic equations of motion with the right-hand side in implicit form. Once reduced to equations of motion with nonholonomic constraints, they allow for the solution of the WMR's forward and inverse dynamics problems. The use of Lagrange equations with multipliers to describe the WMR's dynamics allows to determine the values of friction forces acting at the contact point between the WMR drive wheels and the surface, and thereby to determine whether the desired trajectory can be executed in the rolling without slipping motion. The disadvantage of this approach is in the computational complexity and difficulty in determining the values of Lagrange coefficients, therefore a transformation is applied that allows for decoupling multipliers from the driving moments. The WMR's dynamics may be also described by means of Maggi's mathematical formalism [7, 8, 10]. Thus obtained model, which has a convenient computational form, allows for the calculation of driving moments values for the WMR drive wheels.

Maggi's equations were selected to describe the WMR's dynamics. The motion of dynamic systems expressed by means of Maggi's equations in generalized coordinates is defined as follows

$$\sum_{j=1}^{h} C_{i,j} \left[ \frac{d}{dt} \left( \frac{\partial E}{\partial \dot{q}_j} \right) - \frac{\partial E}{\partial q_j} \right] = \Theta_i \ , \tag{2.22}$$

where $i = 1, \ldots, g$, $g$ – number of independent parameters of the system in generalized coordinates $q_j$, equal to the number of system's degrees of freedom, $j = 1, \ldots, h$, $h$ – number of generalized coordinates, $E = E(\dot{\mathbf{q}})$ – kinetic energy of the system, $C_{i,j}$ – coefficients. The diagram of the WMR is shown in Fig. 2.7.

All generalized velocities are written in the following form

$$\dot{q}_j = \sum_{i=1}^{g} C_{i,j} \dot{e}_i + G_j \ , \tag{2.23}$$

where $\dot{e}_i$ – kinetic parameters of the system in generalized coordinates, $G_j$ – coefficients. The right hand-sides of Eq. (2.22) are the coefficients of variations $\delta \dot{e}_i$

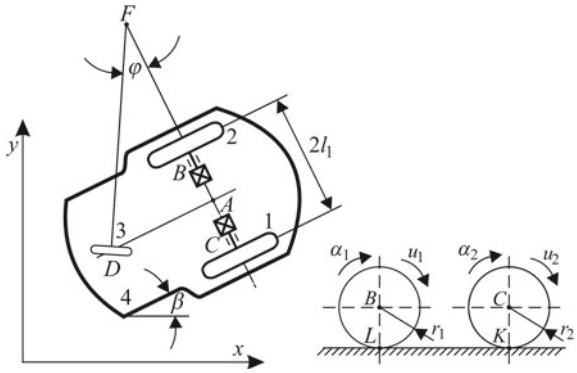



**Fig. 2.7** Diagram of the WMR

in expressions for virtual work of system's external forces. These coefficients are defined as follows [10]

$$\sum_{i=1}^{g} \Theta_i \delta e_i = \sum_{i=1}^{g} \delta e_i \sum_{j=1}^{h} C_{i,j} Q_{Fj} \ , \tag{2.24}$$

where $\mathbf{Q}_F$ – vector of generalized forces, given the driving moments of the WMR wheels 1 and 2, and rolling resistance. Thus formulated Maggi's equations are used to describe the WMR point $A$ motion. It is assumed that robot's motion is executed in a single plane. In order to clearly determine its position and orientation it is necessary to provide the position of point $A$ i.e. coordinates $x_A$, $y_A$ related to the orientation of the frame defined by the instantaneous angle of rotation $\beta$, as well as the rotation angles of drive wheels 1 and 2, denoted by $\alpha_1$ and $\alpha_2$, respectively. Vectors of generalized coordinates and generalized velocities are as follows

$$\mathbf{q} = [x_A, y_A, \beta, \alpha_1, \alpha_2]^T \ , \tag{2.25}$$

$$\dot{\mathbf{q}} = \left[\dot{x}_A, \dot{y}_A, \dot{\beta}, \dot{\alpha}_1, \dot{\alpha}_2\right]^T \ . \tag{2.26}$$

In the analysis of the values of the external forces acting on the examined dynamic system, it is essential to include the dry friction forces which occur in the tangent plane of contact between the drive wheels and the surface. These forces are shown in Fig. 2.8, where $\overline{\mathbf{T}}_{1\tau}$, $\overline{\mathbf{T}}_{2\tau}$ – circumferential dry friction forces, $\overline{\mathbf{T}}_{1n}$, $\overline{\mathbf{T}}_{2n}$ – transverse dry friction forces [7].

The considered WMR is a system with two degrees of freedom. The movement of WMR is analyzed in the $xy$ plane. Given that independent coordinates are represented by drive wheels rotation angles $\alpha_1$ and $\alpha_2$, then the arrangement of velocity vectors with regard to points $A$, $B$ and $C$ implies the following equations for velocities

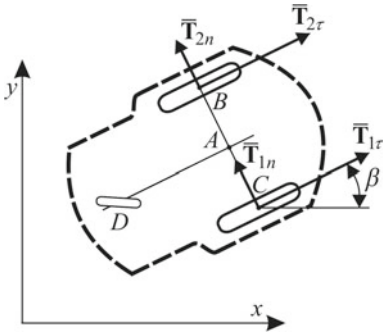



**Fig. 2.8** Friction forces acting on the WMR drive wheels

$$\begin{aligned}
\dot{x}_A &= \frac{r}{2}\left(\dot{\alpha}_1 + \dot{\alpha}_2\right)\cos\left(\beta\right) \ , \\
\dot{y}_A &= \frac{r}{2}\left(\dot{\alpha}_1 + \dot{\alpha}_2\right)\sin\left(\beta\right) \ , \\
\dot{\beta} &= \frac{r}{2l_1}\left(\dot{\alpha}_1 - \dot{\alpha}_2\right) \ .
\end{aligned} \tag{2.27}$$

Based on relation (2.23) generalized velocities are written as follows

$$\begin{aligned}
\dot{q}_1 &= \dot{x}_A = \frac{r}{2}\left(\dot{\alpha}_1 + \dot{\alpha}_2\right)\cos\left(\beta\right) = \frac{r}{2}\left(\dot{e}_1 + \dot{e}_2\right)\cos\left(\beta\right) = C_{1,1}\dot{e}_1 + C_{2,1}\dot{e}_2 + G_1 \ , \\
\dot{q}_2 &= \dot{y}_A = \frac{r}{2}\left(\dot{\alpha}_1 + \dot{\alpha}_2\right)\sin\left(\beta\right) = \frac{r}{2}\left(\dot{e}_1 + \dot{e}_2\right)\sin\left(\beta\right) = C_{1,2}\dot{e}_1 + C_{2,2}\dot{e}_2 + G_2 \ , \\
\dot{q}_3 &= \dot{\beta} = \frac{r}{2l_1}\left(\dot{\alpha}_1 - \dot{\alpha}_2\right) = \frac{r}{2l_1}\left(\dot{e}_1 - \dot{e}_2\right) = C_{1,3}\dot{e}_1 + C_{2,3}\dot{e}_2 + G_3 \ , \\
\dot{q}_4 &= \dot{\alpha}_1 = \dot{e}_1 = C_{1,4}\dot{e}_1 + C_{2,4}\dot{e}_2 + G_4 \ , \\
\dot{q}_5 &= \dot{\alpha}_2 = \dot{e}_2 = C_{1,5}\dot{e}_1 + C_{2,5}\dot{e}_2 + G_5 \ ,
\end{aligned} \tag{2.28}$$

where coefficients $C_{i,j}$ and $G_j$ have the following values

$$\left.\begin{array}{lll}
C_{1,1} = \dfrac{r}{2}\cos\left(\beta\right) \ , & C_{2,1} = \dfrac{r}{2}\cos\left(\beta\right) \ , & G_1 = 0 \ , \\
C_{1,2} = \dfrac{r}{2}\sin\left(\beta\right) \ , & C_{2,2} = \dfrac{r}{2}\sin\left(\beta\right) \ , & G_2 = 0 \ , \\
C_{1,3} = \dfrac{r}{2l_1} \ , & C_{2,3} = -\dfrac{r}{2l_1} \ , & G_3 = 0 \ , \\
C_{1,4} = 1 \ , & C_{2,4} = 0 \ , & G_4 = 0 \ , \\
C_{1,5} = 0 \ , & C_{2,5} = 1 \ , & G_5 = 0 \ .
\end{array}\right\} \tag{2.29}$$

Given the generalized forces described by relation (2.24), and the values of coefficients $C_{i,j}$ (2.29), the WMR's dynamic equations can be written as

$$\begin{aligned}
\Theta_1 &= C_{1,1}Q_{F1} + C_{1,2}Q_{F2} + C_{1,3}Q_{F3} + C_{1,4}Q_{F4} + C_{1,5}Q_{F5} = u_1 - N_1 f_1 \ , \\
\Theta_2 &= C_{2,1}Q_{F1} + C_{2,2}Q_{F2} + C_{2,3}Q_{F3} + C_{2,4}Q_{F4} + C_{2,5}Q_{F5} = u_2 - N_2 f_2 \ .
\end{aligned} \tag{2.30}$$

In the present case, Maggi's equations take the following form

$$\begin{aligned}
&(2m_1+m_4)\left(\frac{r}{2}\right)^2(\ddot{\alpha}_1+\ddot{\alpha}_2)+2m_4\left(\frac{r}{2l_1}\right)^2 rl_2(\dot{\alpha}_2-\dot{\alpha}_1)\dot{\alpha}_2+I_{z1}\ddot{\alpha}_1+\\
&+\left(2m_1l_1^2+m_4l_2^2+2I_{x1}+I_{z4}\right)\frac{r}{2l_1}(\ddot{\alpha}_1-\ddot{\alpha}_2)=u_1-N_1f_1\,,\\
&(2m_1+m_4)\left(\frac{r}{2}\right)^2(\ddot{\alpha}_1+\ddot{\alpha}_2)+2m_4\left(\frac{r}{2l_1}\right)^2 rl_2(\dot{\alpha}_1-\dot{\alpha}_2)\dot{\alpha}_1+I_{z2}\ddot{\alpha}_2+\\
&-\left(2m_1l_1^2+m_4l_2^2+2I_{x1}+I_{z4}\right)\frac{r}{2l_1}(\ddot{\alpha}_1-\ddot{\alpha}_2)=u_2-N_2f_2\,,
\end{aligned} \tag{2.31}$$

where $m_1=m_2$ – substitute masses of WMR drive wheels 1 and 2,
$m_4$ – substitute mass of the WMR's frame,
$I_{x1}=I_{x2}$ – substitute mass moments of inertia of drive wheels 1 and 2 that are determined relative to axes $x_1$ and $x_2$, which relate to the drive wheels, respectively,
$I_{z1}=I_{z2}$ – substitute mass moments of inertia of drive wheels 1 and 2 relative to drive wheels rotation axes,
$I_{z4}$ – substitute mass moment of inertia of the WMR's frame relative to axis $z_4$ that relates to the frame, assuming the axes of the reference frame bounded with a given WMR's part are the central principal axes of inertia,
$N_1$, $N_2$ – normal forces relative to wheels 1 and 2,
$f_1$, $f_2$ – rolling friction coefficients relative to respective WMR wheels,
$u_1$, $u_2$ – driving moments (control signals),
$l, l_1, l_2, h_1$ – respective lengths resulting from the geometry of the system,
$r_1=r_2=r$ – radiuses of respective wheels.

Maggi's equations (2.31) were applied to describe the WMR's dynamics. Their vector/matrix form is shown below [7, 8].

$$\begin{aligned}
&\begin{bmatrix}
(2m_1+m_4)\left(\frac{r}{2}\right)^2+I_{z1}+ & (2m_1+m_4)\left(\frac{r}{2}\right)^2+\\
+\left(2m_1l_1^2+m_4l_2^2+2I_{x1}+I_{z4}\right)\frac{r}{2l_1}\,, & -\left(2m_1l_1^2+m_4l_2^2+2I_{x1}+I_{z4}\right)\frac{r}{2l_1}\\
(2m_1+m_4)\left(\frac{r}{2}\right)^2+ & (2m_1+m_4)\left(\frac{r}{2}\right)^2+I_{z2}+\\
-\left(2m_1l_1^2+m_4l_2^2+2I_{x1}+I_{z4}\right)\frac{r}{2l_1}\,, & +\left(2m_1l_1^2+m_4l_2^2+2I_{x1}+I_{z4}\right)\frac{r}{2l_1}
\end{bmatrix}\begin{bmatrix}\ddot{\alpha}_1\\ \ddot{\alpha}_2\end{bmatrix}\\
&+\begin{bmatrix}
0\,, & 2m_4\left(\frac{r}{2l_1}\right)^2 rl_2(\dot{\alpha}_2-\dot{\alpha}_1)\\
2m_4\left(\frac{r}{2l_1}\right)^2 rl_2(\dot{\alpha}_1-\dot{\alpha}_2)\,, & 0
\end{bmatrix}\begin{bmatrix}\dot{\alpha}_1\\ \dot{\alpha}_2\end{bmatrix}\\
&+\begin{bmatrix}N_1f_1\operatorname{sgn}(\dot{\alpha}_1)\\ N_2f_2\operatorname{sgn}(\dot{\alpha}_2)\end{bmatrix}=\begin{bmatrix}u_1\\ u_2\end{bmatrix}.
\end{aligned} \tag{2.32}$$

The following parameters can be introduced to simplify the WMR's dynamic equations

$$
\begin{aligned}
a_1 &= (2m_1 + m_4)\left(\frac{r}{2}\right)^2 , \\
a_2 &= \left(2m_1 l_1^2 + m_4 l_2^2 + 2I_{x1} + I_{z4}\right)\frac{r}{2l_1} , \\
a_3 &= I_{z1} = I_{z2} , \\
a_4 &= 2m_4\left(\frac{r}{2l_1}\right)^2 r l_2 , \\
a_5 &= N_1 f_1 , \\
a_6 &= N_2 f_2 ,
\end{aligned}
\tag{2.33}
$$

given the above, relation (2.32) can be written as

$$
\mathbf{M}\ddot{\boldsymbol{\alpha}} + \mathbf{C}\left(\dot{\boldsymbol{\alpha}}\right)\dot{\boldsymbol{\alpha}} + \mathbf{F}\left(\dot{\boldsymbol{\alpha}}\right) + \boldsymbol{\tau}_d\left(t\right) = \mathbf{u} , \tag{2.34}
$$

where $\mathbf{M}$ – inertia matrix of the WMR, $\mathbf{C}\left(\dot{\boldsymbol{\alpha}}\right)\dot{\boldsymbol{\alpha}}$ – vector of moments of the centrifugal and Coriolis forces, $\mathbf{F}\left(\dot{\boldsymbol{\alpha}}\right)$ – friction vector, $\boldsymbol{\tau}_d\left(t\right) = \left[\tau_{d1}\left(t\right), \tau_{d2}\left(t\right)\right]^T$ – vector of bounded disturbances - that also relates to the dynamics of the WMR's elements that are not modeled, $\mathbf{u}$ – control vector - that includes control signals in the form of driving moments of respective drive units, $\dot{\boldsymbol{\alpha}} = \left[\dot{\alpha}_1, \dot{\alpha}_2\right]^T$ – angular velocities vector of the WMR drive wheels rotation.

Matrices $\mathbf{M}$, $\mathbf{C}\left(\dot{\boldsymbol{\alpha}}\right)$, and vector $\mathbf{F}\left(\dot{\boldsymbol{\alpha}}\right)$ take the form

$$
\begin{aligned}
\mathbf{M} &= \begin{bmatrix} a_1 + a_2 + a_3 , & a_1 - a_2 \\ a_1 - a_2 , & a_1 + a_2 + a_3 \end{bmatrix} , \\
\mathbf{C}\left(\dot{\boldsymbol{\alpha}}\right) &= \begin{bmatrix} 0 , & a_4\left(\dot{\alpha}_2 - \dot{\alpha}_1\right) \\ -a_4\left(\dot{\alpha}_1 - \dot{\alpha}_2\right) , & 0 \end{bmatrix} , \\
\mathbf{F}\left(\dot{\boldsymbol{\alpha}}\right) &= \begin{bmatrix} a_5 \mathrm{sgn}\left(\dot{\alpha}_1\right) \\ a_6 \mathrm{sgn}\left(\dot{\alpha}_2\right) \end{bmatrix} .
\end{aligned}
\tag{2.35}
$$

Maggi's equations make it possible to circumvent the procedure of decoupling multipliers in Lagrange equations, which is time-consuming for complex dynamic systems. Thus obtained relations allow for the solution of the forward and inverse dynamics problems of the WMR's dynamics.

Equation (2.34) may be written in a linear form with respect to parameters $\mathbf{a}$

$$
\mathbf{Y}\left(\dot{\boldsymbol{\alpha}}, \ddot{\boldsymbol{\alpha}}\right)^T \mathbf{a} + \boldsymbol{\tau}_d\left(t\right) = \mathbf{u} , \tag{2.36}
$$

where $\mathbf{Y}\left(\dot{\boldsymbol{\alpha}}, \ddot{\boldsymbol{\alpha}}\right)$ – so-called regression matrix that takes the form

$$
\mathbf{Y}\left(\dot{\boldsymbol{\alpha}}, \ddot{\boldsymbol{\alpha}}\right) = \begin{bmatrix} \ddot{\alpha}_1 + \ddot{\alpha}_2 , & \ddot{\alpha}_1 , & \ddot{\alpha}_1 - \ddot{\alpha}_2 , & \dot{\alpha}_2^2 - \dot{\alpha}_1\dot{\alpha}_2 , & \mathrm{sgn}\left(\dot{\alpha}_1\right) , & 0 \\ \ddot{\alpha}_1 + \ddot{\alpha}_2 , & \ddot{\alpha}_2 , & \ddot{\alpha}_2 - \ddot{\alpha}_1 , & \dot{\alpha}_1^2 - \dot{\alpha}_1\dot{\alpha}_2 , & 0 , & \mathrm{sgn}\left(\dot{\alpha}_2\right) \end{bmatrix}^T . \tag{2.37}
$$

The nominal set of parameters of the WMR Pioneer 2-DX was adopted and denoted by $\mathbf{a}$, whereas the second set denoted by $\mathbf{a}_d$ refers to the parameters of the WMR carrying a load of $m_{RL} = 4$ [kg]. These parameters were applied to simulate

**Table 2.1** Adopted parameter values for the Pioneer2-DX WMR

| Parameter | Value (no load) ($\mathbf{a}$) | Parameter | Value (load applied) ($\mathbf{a}_d$) | Unit |
|---|---|---|---|---|
| $a_1$ | 0.1207 | $a_{d1}$ | 0.1343 | kgm$^2$ |
| $a_2$ | 0.0768 | $a_{d2}$ | 0.0945 | kgm$^2$ |
| $a_3$ | 0.037 | $a_{d3}$ | 0.037 | kgm$^2$ |
| $a_4$ | 0.001 | $a_{d4}$ | 0.001 | kgm$^2$ |
| $a_5$ | 2.025 | $a_{d5}$ | 2.296 | Nm |
| $a_6$ | 2.025 | $a_{d6}$ | 2.296 | Nm |

disturbances during the movement of the WMR. Both sets of parameters are presented in Table 2.1.

The model of forward dynamics of a mobile robot can be defined based on Eq. (2.34), thus

$$\ddot{\boldsymbol{\alpha}} = \mathbf{M}^{-1}\left[\mathbf{u} - \mathbf{C}\left(\dot{\boldsymbol{\alpha}}\right)\dot{\boldsymbol{\alpha}} - \mathbf{F}\left(\dot{\boldsymbol{\alpha}}\right) - \boldsymbol{\tau}_d\left(t\right)\right] . \tag{2.38}$$

Equation (2.38) will be applied further in this work for the modeling of mobile robot's motion.

A continuous model of the WMR's dynamics (2.38) was discretized with the use of Euler's method of approximation of continuous derivative by a difference (forward rectangular rule). The parameters of motion were computed (in a simulation) or measured (in an experiment) in discrete- time periods $\boldsymbol{\alpha}\left(t_{\{k\}}\right), \dot{\boldsymbol{\alpha}}\left(t_{\{k\}}\right)$, where $t_{\{k\}} = kh$, $k$ – integer indicating an iteration step, $k = 1, \ldots, N$, $N$ – number of iteration steps, $h = t_{\{k+1\}} - t_{\{k\}}$ – time discretization parameter, $\boldsymbol{\alpha}\left(t_{\{k\}}\right)$ and $\boldsymbol{\alpha}\left(t_{\{k+1\}}\right)$ – WMR drive wheels rotation angles in discrete-time periods $t_{\{k\}}$ and $t_{\{k+1\}}$ (for steps $k$ and $k+1$). Substituting $\mathbf{z}_1 = \boldsymbol{\alpha}$, $\mathbf{z}_2 = \dot{\boldsymbol{\alpha}}$ into (2.38), the following discrete description of the WMR's dynamics was obtained

$$\begin{aligned} \mathbf{z}_{1\{k+1\}} &= \mathbf{z}_{1\{k\}} + h\mathbf{z}_{2\{k\}} , \\ \mathbf{z}_{2\{k+1\}} &= \mathbf{z}_{2\{k\}} - h\mathbf{M}^{-1}\left[\mathbf{C}\left(\mathbf{z}_{2\{k\}}\right)\mathbf{z}_{2\{k\}} + \mathbf{F}\left(\mathbf{z}_{2\{k\}}\right) + \boldsymbol{\tau}_{d\{k\}} - \mathbf{u}_{\{k\}}\right] , \end{aligned} \tag{2.39}$$

where $\mathbf{z}_{1\{k\}} = \left[z_{11\{k\}}, z_{12\{k\}}\right]^T$ – vector of discrete drive wheels rotation angles that corresponds to the continuous vector $\boldsymbol{\alpha}$, $\mathbf{z}_{2\{k\}} = \left[z_{21\{k\}}, z_{22\{k\}}\right]^T$ – vector of discrete angular velocities that corresponds to the continuous vector $\dot{\boldsymbol{\alpha}}$.

Difference equations of mobile robot's dynamics (2.39) that were derived by means of Maggi's equations will be used further in this work for the modeling of motion of a controlled object, while a discrete form of relation (2.34) was applied in the synthesis of robot's tracking control algorithms.

The structural properties of the WMR's dynamic model (2.34) are used in the synthesis of tracking control algorithms. These properties are presented below.

**Structural Properties of the WMR's Mathematical Model**
Description of the WMR's dynamics in the form of Eq. (2.34) meets the following assumptions [6, 11, 14]:

1. Inertia matrix $\mathbf{M}$ is symmetric and positive-definite, and meets the constraints
$$\sigma_{\min}(\mathbf{M})\,\mathbf{I} \leq \mathbf{M} \leq \sigma_{\max}(\mathbf{M})\,\mathbf{I}\,, \tag{2.40}$$
where $\mathbf{I}$ – identity matrix, $\sigma_{\min}(\mathbf{M})$, $\sigma_{\max}(\mathbf{M})$ – respectively, minimum and maximum strictly positive eigenvalue of the inertia matrix.
2. Matrix $\mathbf{C}(\dot{\boldsymbol{\alpha}})$ is such that the matrix
$$\mathbf{S}(\dot{\boldsymbol{\alpha}}) = \dot{\mathbf{M}} - 2\mathbf{C}(\dot{\boldsymbol{\alpha}})\,, \tag{2.41}$$
is skew-symmetric. Thus the following relation
$$\boldsymbol{\xi}^T \mathbf{S}(\dot{\boldsymbol{\alpha}})\,\boldsymbol{\xi} = \mathbf{0}\,, \tag{2.42}$$
where $\boldsymbol{\xi}$ – any given vector of appropriate dimension.
3. Vector of disturbances $\boldsymbol{\tau}_d(t)$ acting on the WMR is bounded so that $\|\tau_{dj}(t)\| \leq b_{dj}$, where $b_{dj}$ is a positive constant, $j = 1, 2$.
4. The WMR's dynamic Eq. (2.34) can be written in a linear form with respect to the parameters, hence
$$\mathbf{M}\ddot{\boldsymbol{\alpha}} + \mathbf{C}(\dot{\boldsymbol{\alpha}})\,\dot{\boldsymbol{\alpha}} + \mathbf{F}(\dot{\boldsymbol{\alpha}}) + \boldsymbol{\tau}_d(t) = \mathbf{Y}(\dot{\boldsymbol{\alpha}}, \ddot{\boldsymbol{\alpha}})^T\,\mathbf{a} + \boldsymbol{\tau}_d(t) = \mathbf{u}\,, \tag{2.43}$$
vector of parameters $\mathbf{a}$ shall consist of a minimum number of linearly independent elements.

#### 2.1.2.1 Simulation of Inverse Dynamics Problem – The WMR's Motion on a Closed-Loop Path

In the simulation of the WMR's motion the robot's characteristic point $A$ follows the desired trajectory with a loop path. The inverse kinematics solution trajectory from Sect. 2.1.1.1 was applied. Based on the values of the desired WMR's parameters such as angular velocities $(\dot{\alpha}_1, \dot{\alpha}_2)$ and angular accelerations $(\ddot{\alpha}_1, \ddot{\alpha}_2)$, and according to Eq. (2.34) control signals $u_1$ and $u_2$ were generated. The control signals determine the WMR's motion on the desired path given the desired angular velocities and accelerations of the drive wheels. The nominal values of the WMR's model parameters $\mathbf{a}$ were adopted, in accordance with Table 2.1.

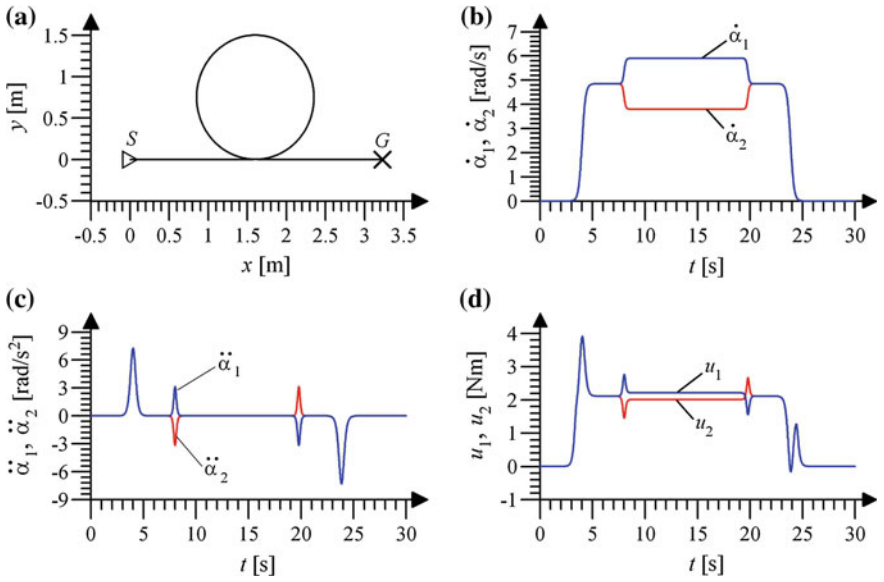



**Fig. 2.9** **a** Desired path of point $A$ on the WMR, **b** angular velocities $\dot{\alpha}_1$ and $\dot{\alpha}_2$, **c** angular accelerations $\ddot{\alpha}_1$ and $\ddot{\alpha}_2$, **d** control signals $u_1$, $u_2$

The diagram of the desired motion path of point $A$ is shown in Fig. 2.9a, desired angular velocities of the drive wheels ($\dot{\alpha}_1$, $\dot{\alpha}_2$) and angular accelerations ($\ddot{\alpha}_1$, $\ddot{\alpha}_2$) are illustrated in Fig. 2.9b, c, respectively. Figure 2.9d presents the generated control signals.

It can be noted that the waveforms shown in Fig. 2.9d directly correspond to the phases of motion related to the desired trajectory. At the initial time, the position of the WMR's point $A$ is at point $S$. In the acceleration period ($t \in < 3, 5 >$) the control signals are generated, thereby initializing the motion of robot's mass despite robot's innate inertia and resistance to motion. Hence, the highest values of control signals $u_1$ and $u_2$ are observed in this phase of motion. In the next phase, which is the constant motion on a rectilinear path ($t \in < 5, 7.5 >$), the values of angular accelerations are equal to zero, thus in accordance with Eq. (2.34) the values of control signals are determined merely by the modeled effects related to the resistance to motion. Another phase is the motion along a circular path (with radius $R = 0.75$ [m]) preceded by the curve entrance transition phase and completed with the curve exit transition phase. The curve entrance requires an increase in the angular velocity of wheel 1 and a decrease in the angular velocity of wheel 2 which results in the increase in the value of control signal $u_1$ and the decrease in the value of control signal $u_2$ in $t \in < 7.5, 8.5 >$. In the constant motion on a circular path ($t \in < 7.5, 20.5 >$) the control signals are affected by the vector of moments of the centrifugal and Coriolis forces, thus the different values of drive wheels control signals in this phase of motion. The curve exit phase is followed by another phase of constant motion on a rectilinear

path ($t \in < 20.5, 23 >$). The final phase of motion is braking ($t \in < 23, 25 >$) and complete stop at point $G$, where the angular velocities tend to zero and the control signals go to zero as well.

#### 2.1.2.2 Simulation of Inverse Dynamics Problem – The WMR's Motion on an 8-Shaped Path

In the simulation of the WMR's motion the robot's characteristic point $A$ moves on an 8-shaped path. The inverse kinematics solution trajectory from Sect. 2.1.1.2 was used. The simulation conditions applied are those from Sect. 2.1.2.1. The diagram of the defined motion path of point $A$ is shown in Fig. 2.10a, desired angular velocities of the drive wheels ($\dot{\alpha}_1$, $\dot{\alpha}_2$) and angular accelerations ($\ddot{\alpha}_1$, $\ddot{\alpha}_2$) are illustrated in Fig. 2.10b, c, respectively. Figure 2.10d presents the generated control signals.

The desired trajectory consists of two main periods. The first one consists in point $A$'s motion on a rectilinear path from its initial position at point $S$, followed by the motion along a curved path in the leftward direction, curve exit and the rectilinear motion with braking and stop at point $P$. The second main period of motion begins at point $P$ and consists in the rectilinear motion, followed by the motion on a curved path in the rightward direction and the rectilinear motion with braking and stop at point $G$. Each of these two main periods consists of analogous phases to those described in Sect. 2.1.2.1 except that during the motion on a curved path there is

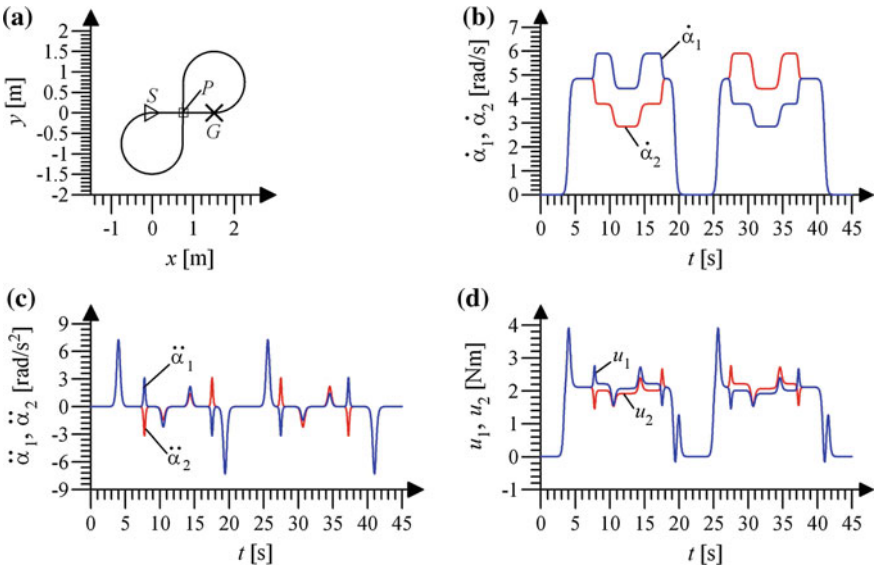



**Fig. 2.10** **a** Desired path of point $A$ on the WMR, **b** angular velocities $\dot{\alpha}_1$ and $\dot{\alpha}_2$, **c** angular accelerations $\ddot{\alpha}_1$ and $\ddot{\alpha}_2$, **d** control signals $u_1$, $u_2$

an additional decrease in point $A$'s velocity from $v_A = 0.4\left[\frac{m}{s}\right]$ to $v_A = 0.3\left[\frac{m}{s}\right]$ in the periods $t \in < 10, 15 >$ [s] and $t \in < 30, 35 >$ [s]. The decrease in the values of angular velocities of drive wheels rotation in the aforementioned periods, results in the lower values of the control signals.

## 2.2 Robotic Manipulator

Scorbot–ER 4pc is a laboratory robotic manipulator (RM) with five degrees of freedom comprising revolute kinematic pairs of the arm and wrist. The robot was designed and developed to emulate an industrial robot, however its unique feature is the open mechanical structure that allows to observe the movement of the arm mechanisms and the open structure of the control system. Scorbot–ER 4pc [17] RM is shown in Fig. 2.11a, and its structure is illustrated by means of a schematic diagram in Fig. 2.11b.

The gripper is the robot's end-effector that can reach the desired position through the movement of the robot arm with three degrees of freedom. Another two degrees of freedom allow the gripper to be oriented arbitrarily and a servo motor allows closing of the gripper jaws. The robot is driven by drive units that comprise 12 [V] DC motors, gears and incremental encoders. Reduction gears were installed with ratios of $i_1 = i_2 = i_3 = 1 : 127.1$ in the drive units of links 1, 2 and 3, and ratios of $i_4 = i_5 = 1 : 65.5$ in the drive units of links 4 and 5. The motors that drive link 2 (upper arm), 3 (forearm) and the gripper are mounted in link 1 (base), thus they do not weigh down the links, whose masses and mass moments of inertia are relatively small. The power is transmitted by cogbelts, whose flexibility has a marginal impact on the robot arm movement given the position of the drive units in link 1. Robot's payload capacity is $m_L = 1$ [kg], including gripper, and the robot mass is $m_R = 11.5$ [kg].

The open structure of manipulator's control system along with dSpace measurement and diagnostic tools allow for experimental verification of different methods for modeling and control of RMs. Research on the synthesis of control algorithms with regard to the motion of dynamic systems requires knowledge of the system's

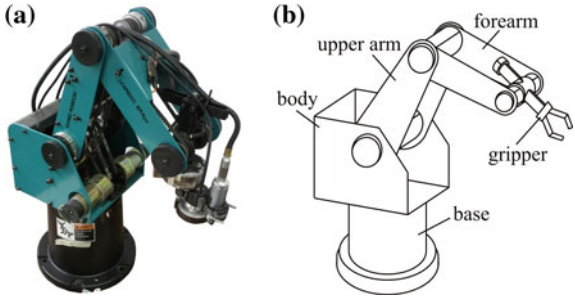



**Fig. 2.11** **a** Scorbot-ER 4pc robotic manipulator, **b** schematic diagram of the robotic manipulator

mathematical model that should be simple, namely, consider solely the most important effects. Therefore, the following assumptions are made [23]:

- analyzed kinematic chain of the manipulator has three degrees of freedom, gripper movements are negligible,
- manipulator links were modeled as rigid bodies,
- gripper was modeled as mass concentrated at point $C$, at the end of the robotic arm,
- flexibility and backlash in gears are negligible,
- dynamics of actuators was not considered, due to short time constants of motors,
- link 1 was modeled as a cylinder,
- links 2 and 3 were assumed to have axes of symmetry which intersect the axes of their respective joints.

### 2.2.1 Description of the Kinematics of a Robotic Manipulator

The issues related to the kinematics of robotic manipulators include forward and inverse kinematics problems. A problem-solving approach to forward kinematics consists in the determination of the tool center point (TCP) position and tool orientation within the manipulator's workspace, taking into account the joint coordinates (configuration coordinates). To solve the inverse kinematics problem joints' coordinates, velocities and accelerations must be determined based on the assumed motion of the tool within the workspace. From a mathematical point of view solving the inverse kinematics problem is more difficult than solving the problem of forward kinematics, however it is more important in terms of robotics. An analysis of the inverse kinematics problem is carried out to determine the trajectory which is to be executed by the tracking control system [23]. Except in extraordinary cases, solving the inverse kinematics problem is difficult, which is due to ambiguity of solutions, discontinuity in solutions and kinematic singularity.

This subchapter describes the kinematics of the Scorbot - ER 4pc RM by means of the Denavit–Hartenberg notation (D–H) [2, 9, 15, 16, 19, 20] which employs homogenous coordinates and transformation matrices [15, 16, 19]. The Scorbot - ER 4pc's arm has a joint kinematic structure (anthropomorphic). According to the adopted D-H notation, the $i$th coordinate frame is attached to each $i$th link of the manipulator's kinematic chain. The homogenous transformation matrix $\mathbf{A}_{i-1}^{i}$ transforms coordinates of a selected point from the $i$th coordinate system into the $i-1$ system. It is obtained by combining four transformations [19], according to the relation

$$\mathbf{A}_{i-1}^{i} = \mathbf{Rot}_{z,\Theta i}\mathbf{Trans}_{z,di}\mathbf{Trans}_{x,ai}\mathbf{Rot}_{x,\alpha i} \ , \tag{2.44}$$

where individual matrices of rotation and translation express the angle of rotation and displacement of the $i$th system to the $i-1$ system, $\mathbf{Rot}_{z,\Theta i}$ is the matrix of rotation through angle $\Theta_i$ about axis $z$, expressed by the relation

$$\mathbf{Rot}_{z,\Theta i} = \begin{bmatrix} \cos(\Theta_i) & -\sin(\Theta_i) & 0 & 0 \\ \sin(\Theta_i) & \cos(\Theta_i) & 0 & 0 \\ 0 & 0 & 1 & 0 \\ 0 & 0 & 0 & 1 \end{bmatrix}, \tag{2.45}$$

translation matrix $\mathbf{Trans}_{z,di}$ expresses translation along axis $z$ by distance $d_i$, according to the relation

$$\mathbf{Trans}_{z,di} = \begin{bmatrix} 1 & 0 & 0 & 0 \\ 0 & 1 & 0 & 0 \\ 0 & 0 & 1 & d_i \\ 0 & 0 & 0 & 1 \end{bmatrix}, \tag{2.46}$$

translation matrix $\mathbf{Trans}_{x,ai}$ expresses translation along axis $x$ by distance $a_i$

$$\mathbf{Trans}_{x,ai} = \begin{bmatrix} 1 & 0 & 0 & a_i \\ 0 & 1 & 0 & 0 \\ 0 & 0 & 1 & 0 \\ 0 & 0 & 0 & 1 \end{bmatrix}, \tag{2.47}$$

and rotation matrix $\mathbf{Rot}_{x,\alpha i}$ expresses rotation through angle $\alpha_i$ relative to axis $x$, according to the relation

$$\mathbf{Rot}_{x,\alpha i} = \begin{bmatrix} 1 & 0 & 0 & 0 \\ 0 & \cos(\alpha_i) & -\sin(\alpha_i) & 0 \\ 0 & \sin(\alpha_i) & \cos(\alpha_i) & 0 \\ 0 & 0 & 0 & 1 \end{bmatrix}, \tag{2.48}$$

where the parameters of the $i$th link of the kinematic chain are: $\Theta_i$ – joint's angle of rotation, $d_i$ – joint offset, $a_i$ - link length, $\alpha_i$ – link twist angle. The application of D-H notation requires the following selection of coordinate frames attached to the links matrix [19]:

- axis $x_i$ of the $i$th coordinate system is perpendicular to axis $z_{i-1}$ of the $i-1$ coordinate system,
- axis $x_i$ of the $i$th coordinate system intersects axis $z_{i-1}$ of the $i-1$ coordinate system,

where parameters $\Theta_i$, $d_i$, $a_i$ and $\alpha_i$ are unambiguously determined and satisfy the relation (2.44).

Finally, matrix $\mathbf{A}_{i-1}^{i}$ has the form

$$\mathbf{A}_{i-1}^{i} = \begin{bmatrix} \cos(\Theta_i) & -\sin(\Theta_i)\cos(\alpha_i) & \sin(\Theta_i)\sin(\alpha_i) & a_i\cos(\Theta_i) \\ \sin(\Theta_i) & \cos(\Theta_i)\cos(\alpha_i) & -\cos(\Theta_i)\sin(\alpha_i) & a_i\sin(\Theta_i) \\ 0 & \sin(\alpha_i) & \cos(\alpha_i) & d_i \\ 0 & 0 & 0 & 1 \end{bmatrix}. \tag{2.49}$$

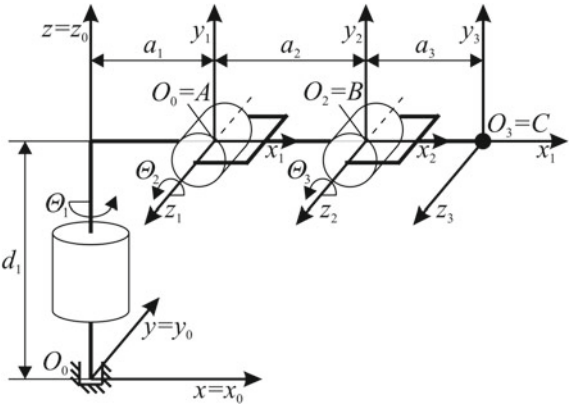



**Fig. 2.12** Schematic diagram of the Scorbot-ER 4pc robotic manipulator with coordinate systems and Devanit–Hartenberg parameters

**Table 2.2** Scorbot-ER 4pc kinematic parameters relevant to Denavit–Hartenberg notation

| Czon | $\Theta_i$ [rad] | $a_i$ [m] | $d_i$ [m] | $\alpha_i$ [rad] |
|---|---|---|---|---|
| 1 | $\Theta_1$ | $l_1 = 0.026$ | $d_1 = 0.35$ | $\pi/2$ |
| 2 | $\Theta_2$ | $l_2 = 0.22$ | 0 | 0 |
| 3 | $\Theta_3$ | $l_3 = 0.22$ | 0 | 0 |

Figure 2.12 shows a schematic diagram of RM structure with kinematic parameters relevant to the D-H notation.

Relevant kinematic parameters of the links are presented in Table 2.2.

Homogenous transformation matrices of the Scorbot-ER 4pc RM [9, 23] take the form:

$$\mathbf{A}_0^1(\Theta_1) = \begin{bmatrix} \cos(\Theta_1) & 0 & \sin(\Theta_1) & l_1\cos(\Theta_1) \\ \sin(\Theta_1) & 0 & -\cos(\Theta_1) & l_1\sin(\Theta_1) \\ 0 & 1 & 0 & d_1 \\ 0 & 0 & 0 & 1 \end{bmatrix}, \tag{2.50}$$

$$\mathbf{A}_1^2(\Theta_2) = \begin{bmatrix} \cos(\Theta_2) & 0 & -\sin(\Theta_2) & l_2\cos(\Theta_2) \\ \sin(\Theta_2) & 0 & \cos(\Theta_2) & l_2\sin(\Theta_2) \\ 0 & 0 & 1 & 0 \\ 0 & 0 & 0 & 1 \end{bmatrix}, \tag{2.51}$$

$$\mathbf{A}_2^3(\Theta_3) = \begin{bmatrix} \cos(\Theta_3) & 0 & -\sin(\Theta_3) & l_3\cos(\Theta_3) \\ \sin(\Theta_3) & 0 & \cos(\Theta_3) & l_3\sin(\Theta_3) \\ 0 & 0 & 1 & 0 \\ 0 & 0 & 0 & 1 \end{bmatrix}. \tag{2.52}$$

Considering the mechanical structure of the manipulator and the methods for measuring rotation angles of the Scorbot-ER 4pc manipulator's links, a new vector of configuration coordinates was adopted

$$\mathbf{q} = \begin{bmatrix} q_1 \\ q_2 \\ q_3 \end{bmatrix} = \begin{bmatrix} \Theta_1 \\ \Theta_2 \\ \Theta_2 + \Theta_3 \end{bmatrix}, \tag{2.53}$$

and new homogenous transformation matrices defined by coordinates $q_i$ in the form

$$\mathbf{A}_0^1(q_1) = \begin{bmatrix} \cos(q_1) & 0 & \sin(q_1) & l_1 \cos(q_1) \\ \sin(q_1) & 0 & -\cos(q_1) & l_1 \sin(q_1) \\ 0 & 1 & 0 & d_1 \\ 0 & 0 & 0 & 1 \end{bmatrix}, \tag{2.54}$$

$$\mathbf{A}_1^2(q_2) = \begin{bmatrix} \cos(q_2) & 0 & -\sin(q_2) & l_2 \cos(q_2) \\ \sin(q_2) & 0 & \cos(q_2) & l_2 \sin(q_2) \\ 0 & 0 & 1 & 0 \\ 0 & 0 & 0 & 1 \end{bmatrix}, \tag{2.55}$$

$$\mathbf{A}_2^3(q_2, q_3) = \begin{bmatrix} \cos(q_3 - q_2) & 0 & -\sin(q_3 - q_2) & l_3 \cos(q_3 - q_2) \\ \sin(q_3 - q_2) & 0 & \cos(q_3 - q_2) & l_3 \sin(q_3 - q_2) \\ 0 & 0 & 1 & 0 \\ 0 & 0 & 0 & 1 \end{bmatrix}, \tag{2.56}$$

that will be used further in this work to determine the manipulator Jacobian.

Transformation of the $j$th coordinate system to the $i-1$ system is defined by matrix $\mathbf{T}_{i-1}^j \in \Re^{4x4}$ expressed in the form [20]:

$$\mathbf{T}_{i-1}^j = \prod_{k=i}^{j} \mathbf{A}_{k-1}^k(\mathbf{q}), \tag{2.57}$$

whose general form is

$$\mathbf{T}_{i-1}^j = \left[\begin{array}{c|c} \mathbf{R}_{i-1}^j & \mathbf{p}_{i-1}^j \\ \hline \mathbf{0} & 1 \end{array}\right], \tag{2.58}$$

where $\mathbf{R}_{i-1}^j \in \Re^{3x3}$ – matrix of rotation of the $j$th coordinate system relative to the $i-1$ system, $\mathbf{p}_{i-1}^j \in \Re^{3x1}$ – vector of translation of the $j$th coordinate system relative to the $i-1$ system.

The Jacobian matrix (in robotics also referred to as the Jacobian) is essential for the modeling, motion planning and RM control. Scientific publications provide several different types of the Jacobian [19, 20], this monograph only presents the analytical Jacobian [19, 20, 23].

The analytical Jacobian of the RM is derived from the so-called kinematic functions, where the joint coordinates (configuration coordinates) $\mathbf{q}$ are related to the task coordinates $\mathbf{y}$ of manipulator's link e.g. tool position and orientation in robot's task space.

The task coordinates are defined by the relation

$$\mathbf{y} = \mathbf{k}(\mathbf{q}) \ , \tag{2.59}$$

where $\mathbf{k}(\mathbf{q}) \in \Re^{mx1}$ – the so-called kinematic function, $\mathbf{q} \in \Re^{nx1}$ – vector of configuration coordinates, $m$ – dimension of manipulator's task space, $n$ – dimension of manipulator's configuration space.

The connection between the values of velocities in the configuration space and the values of joint velocities is expressed by means of the analytical Jacobian, according to the following relation

$$\dot{\mathbf{y}} = \mathbf{J}(\mathbf{q})\,\dot{\mathbf{q}} \ , \tag{2.60}$$

$\dot{\mathbf{y}} \in \Re^{mx1}$ – velocity vector in task coordinates, $\dot{\mathbf{q}} \in \Re^{nx1}$ – vector of configuration velocities, $\mathbf{J}(\mathbf{q}) \in \Re^{mxn}$ – analytical Jacobian expressed in the form

$$\mathbf{J}(\mathbf{q}) = \frac{\partial \mathbf{k}(\mathbf{q})}{\partial \mathbf{q}} \ . \tag{2.61}$$

The selection of manipulator's task coordinates $\mathbf{y}$ has a significant impact on the dimension and form of the Jacobian [19, 20, 23]. The analytical Jacobian of $n$-link manipulator consists of columns $\mathbf{J}_i$, $i = 1, 2, \ldots, n$, that is

$$\mathbf{J}(\mathbf{q}) = [\mathbf{J}_1 \ \ldots \ \mathbf{J}_i \ \ldots \ \mathbf{J}_n] \ , \tag{2.62}$$

where the $i$th column of the revolute joint Jacobian matrix is expressed by

$$\mathbf{J}_i = \begin{bmatrix} \mathbf{R}_{0\ 3^{th}\ col}^{i-1} \times \left(\mathbf{p}_0^n - \mathbf{p}_0^{i-1}\right) \\ \mathbf{R}_{0\ 3^{th}\ col}^{i-1} \end{bmatrix} \ , \tag{2.63}$$

and for a prismatic joint by

$$\mathbf{J}_i = \begin{bmatrix} \mathbf{R}_{0\ 3^{th}\ col}^{i-1} \\ \mathbf{0} \end{bmatrix} \ , \tag{2.64}$$

where $\mathbf{R}_{0\ 3^{th}\ col}^{i-1}$ – is the third column of the rotation matrix resulting from relation (2.58).

The analytical Jacobian of the Scorbot-ER 4pc was determined assuming a 6-dimensional task space, where point $C$ coordinates of the manipulator's kinematic chain $\mathbf{y} = [y_1 y_2 y_3 y_4 y_5 y_6]^T$ describe the position $(y_1, y_2, y_3)$ and the orientation $(y_4, y_5, y_6)$ of the end-effector with respect to the base coordinate system. By applying configuration coordinates (2.53), the analytical Jacobian (2.61) has the form

$$\mathbf{J}(\mathbf{q}) = \begin{bmatrix} -(l_1 + l_2\cos(q_2) + l_3\cos(q_3))\sin(q_1) & -l_2\sin(q_2)\cos(q_1) & -l_3\sin(q_3)\cos(q_1) \\ (l_1 + l_2\cos(q_2) + l_3\cos(q_3))\cos(q_1) & -l_2\sin(q_2)\sin(q_1) & -l_3\sin(q_3)\sin(q_1) \\ 0 & l_2\cos(q_2) & l_3\cos(q_3) \\ 0 & 0 & \sin(q_1) \\ 0 & 0 & -\cos(q_1) \\ 1 & 0 & 0 \end{bmatrix}. \tag{2.65}$$

Another important issue in the analysis of manipulator's kinematics is to determine singular configurations based on the analysis of the Jacobian [20, 23]. The theory indicates that if the manipulator's number of degrees of freedom is lower than the number of task space dimensions, the manipulator has only singular configurations. In this analysis, 6-dimensional task space was adopted for a manipulator with three coordinates in the configuration space (2.53). A manipulator thus defined allows the end-effector to either reach the desired position, in that case the end-effector's orientation depends on the position, or to reach the desired orientation, then the position depends on the orientation. The determination of singular configurations of the Scorbot-ER 4pc manipulator is described in detail in [23].

#### 2.2.1.1 Inverse Kinematics Problem

The following considerations are limited to the first three degrees of freedom of the kinematic chain. Under this assumption the Scorbot-ER 4pc RM is not capable of reaching any arbitrary position and orientation within the 6-dimensional task space. Further considerations deal with the position kinematics which comes down to the division of task coordinates into coordinates $\mathbf{y}_p = [y_1, y_2, y_3]^T$ that relate to the position of the end-effector and coordinates $\mathbf{y}_o = [y_4, y_5, y_6]^T$ that relate to the orientation [23].

A similar division may be made for the analytical Jacobian (2.65) where $\mathbf{J}_p \in \Re^{3x3}$ is the part related to the position

$$\mathbf{J}_p(\mathbf{q}) = \begin{bmatrix} -(l_1 + l_2\cos(q_2) + l_3\cos(q_3))\sin(q_1) & -l_2\sin(q_2)\cos(q_1) & -l_3\sin(q_3)\cos(q_1) \\ (l_1 + l_2\cos(q_2) + l_3\cos(q_3))\cos(q_1) & -l_2\sin(q_2)\sin(q_1) & -l_3\sin(q_3)\sin(q_1) \\ 0 & l_2\cos(q_2) & l_3\cos(q_3) \end{bmatrix}, \tag{2.66}$$

and $\mathbf{J}_o \in \Re^{3x3}$ is the part related to the orientation of the manipulator's end-effector

$$\mathbf{J}_o(\mathbf{q}) = \begin{bmatrix} 0 & 0 & \sin(q_1) \\ 0 & 0 & -\cos(q_1) \\ 1 & 0 & 0 \end{bmatrix}. \tag{2.67}$$

The relation between the velocities of end-effector's point $C$ and the joint velocities of the manipulator is given by

$$\dot{\mathbf{y}}_p = \mathbf{J}_p(\mathbf{q})\,\dot{\mathbf{q}}\,. \tag{2.68}$$

The problems of forward and inverse kinematics of the RM can be solved by means of Eq. (2.68). However, solving the inverse kinematics problem is difficult, which is due to the singularity of manipulator's kinematics as well as the ambiguity and discontinuity in solutions. When solved, it provides the desired trajectory that is necessary for the tracking control of a RM.

The following considerations concern solution of the inverse kinematics problem of a RM, given the desired motion path and velocity of the end-effector's point $C$. In the general case point $C$'s motion path is a curve, defined in the task space

$$\begin{cases} f_1(x_C, z_C) = 0\,, \\ f_2(x_C, y_C) = 0\,, \end{cases} \tag{2.69}$$

where $x_C$, $y_C$, $z_C$ – end-effector's point $C$ coordinates in the base coordinate system $xyz$, corresponding to the position coordinates $\mathbf{y}_p$. The velocity vector of point $C$ has the form

$$\mathbf{v}_C = \begin{bmatrix} \dot{x}_C \\ \dot{y}_C \\ \dot{z}_C \end{bmatrix} = \dot{\mathbf{y}}_p\,, \tag{2.70}$$

whose value is expressed by the relation

$$v_C = \sqrt{\dot{x}_C^2 + \dot{y}_C^2 + \dot{z}_C^2}\,. \tag{2.71}$$

The direction of the velocity vector of point $C$ must be tangent to the path of motion, thus the following relations must be satisfied

$$\begin{cases} \operatorname{grad} f_1(x_C, z_C)\,\mathbf{v}_C = 0\,, \\ \operatorname{grad} f_2(x_C, y_C)\,\mathbf{v}_C = 0\,, \end{cases} \tag{2.72}$$

which can be written as

$$\begin{cases} \begin{bmatrix} \frac{\partial f_1(x_C,z_C)}{\partial x_C} & \frac{\partial f_1(x_C,z_C)}{\partial y_C} & \frac{\partial f_1(x_C,z_C)}{\partial z_C} \end{bmatrix} \begin{bmatrix} \dot{x}_C \\ \dot{y}_C \\ \dot{z}_C \end{bmatrix} = 0\,, \\ \begin{bmatrix} \frac{\partial f_2(x_C,y_C)}{\partial x_C} & \frac{\partial f_2(x_C,y_C)}{\partial y_C} & \frac{\partial f_2(x_C,y_C)}{\partial z_C} \end{bmatrix} \begin{bmatrix} \dot{x}_C \\ \dot{y}_C \\ \dot{z}_C \end{bmatrix} = 0\,. \end{cases} \tag{2.73}$$

Given that $f_{1x} = \frac{\partial f_1(x_C,z_C)}{\partial x_C}$, $f_{1y} = \frac{\partial f_1(x_C,z_C)}{\partial y_C}$, $f_{1z} = \frac{\partial f_1(x_C,z_C)}{\partial z_C}$, $f_{2x} = \frac{\partial f_2(x_C,y_C)}{\partial x_C}$, $f_{2y} = \frac{\partial f_2(x_C,y_C)}{\partial y_C}$, $f_{2z} = \frac{\partial f_2(x_C,y_C)}{\partial z_C}$, solution of Eqs. (2.71) and (2.73) take the form

$$\begin{cases} \dot{x}_C = \mp v_C \frac{f_{1y} f_{2z} - f_{1z} f_{2y}}{\sqrt{(f_{1x} f_{2y} - f_{2x} f_{1y})^2 + (f_{1x} f_{2z} - f_{2x} f_{1z})^2 + (f_{1y} f_{2z} - f_{2y} f_{1z})^2}} , \\ \dot{y}_C = \pm v_C \frac{f_{1x} f_{2z} - f_{1z} f_{2x}}{\sqrt{(f_{1x} f_{2y} - f_{2x} f_{1y})^2 + (f_{1x} f_{2z} - f_{2x} f_{1z})^2 + (f_{1y} f_{2z} - f_{2y} f_{1z})^2}} , \\ \dot{z}_C = \mp v_C \frac{f_{1x} f_{2y} - f_{1y} f_{2x}}{\sqrt{(f_{1x} f_{2y} - f_{2x} f_{1y})^2 + (f_{1x} f_{2z} - f_{2x} f_{1z})^2 + (f_{1y} f_{2z} - f_{2y} f_{1z})^2}} . \end{cases} \tag{2.74}$$

By solving the set of differential equations (2.74) including the initial conditions and pre-determined value of point $C$ velocity vector, it is possible to determine the values of point $C$ velocity vector components with respect to time, as well as the coordinates $x_C$, $y_C$ i $z_C$. Relation (2.68) can be transformed into

$$\dot{\mathbf{q}} = \left[\mathbf{J}_p(\mathbf{q})\right]^{-1} \dot{\mathbf{y}}_p . \tag{2.75}$$

By solving differential equations (2.75) based on the pre-defined values of point $C$ velocity components, it is possible to determine the values of angular velocities and rotation angles of manipulator's links, with respect to time. Differentiating the values of angular velocities provides the values of angular accelerations. Thus obtained variables may constitute the desired reference trajectory to be tracked by the control system. To avoid singular configurations, for which no inverse of the Jacobian $\mathbf{J}_p(\mathbf{q})$, exists, the end-effector's motion path must be properly planned.

#### 2.2.1.2 Simulation of Inverse Kinematics Problem with a Semicircle Path

Following example presents a solution to the inverse kinematics problem with regard to the RM. The assumed path of motion of point $C$ attached to the end-effector has the shape of a semicircle, with center $E$ and radius $R$, and lies in the $xy$ plane.

Thus, it is assumed that there is no motion in the $z$-axis direction, hence the coordinate $z_C = \text{const.}$, and point $C$ velocity relative to $z$-axis is $\dot{z}_C = 0$. The assumed equation for point $C$ motion path is

$$\begin{gathered} (x_C - x_E)^2 + (y_C - y_E)^2 - R^2 = 0 , \\ z_C - d_1 = 0 , \end{gathered} \tag{2.76}$$

where $x_E$, $y_E$ – coordinates of point $E$ (center of the circle), $x_E = 0.36$ [m], $y_E = 0$ [m], $R$ – circle radius, $R = 0.1$ [m]. The assumed value of point $C$ velocity vector is expressed by the following relation

$$v_C = v_C^* \cdot \sum_{m=0}^{5} \frac{(-1)^m}{\left(1 + \exp^{-c_1(t - t_{1+2m})}\right)\left(1 + \exp^{c_1(t - t_{2+2m})}\right)} , \tag{2.77}$$

where $v_C^*$ – maximum velocity of end-effector's point $C$, $v_C^* = 0.08$ [m/s], $c_1$ – slope coefficient of unipolar sigmoid function, $c_1 = 10$ [1/s], $t \in < 0, 40 >$ [s], $t_{1+2m}$ –

mean start-time of $m$th period of acceleration, $t_{2+2m}$ – mean start-time of $m$th period of braking, $m = 0, \ldots, 5, t_1 = 4$ [s], $t_2 = 7.93$ [s], $t_3 = 10$ [s], $t_4 = 13.93$ [s], $t_5 = 16$ [s], $t_6 = 19.93$ [s], $t_7 = 22$ [s], $t_8 = 25.93$ [s], $t_9 = 28$ [s], $t_{10} = 31.93$ [s], $t_{11} = 34$ [s], $t_{12} = 37.93$ [s].

The velocity profile described by relation (2.77) approximates the triangular velocity profile; it was applied to eliminate discontinuities in angular accelerations of trajectory with a triangular velocity profile. In the presented case $f_{1x} = 2\,(x_C - x_E)$, $f_{1y} = 2y_C$, $f_{1z} = f_{2x} = f_{2y} = 0$, $f_{2z} = 1$, and the set of Eq. (2.74) takes a simplified form

$$\begin{cases} \dot{x}_C = \mp v_C \frac{f_{1y}}{\sqrt{f_{1x}^2 + f_{1y}^2}} , \\ \dot{y}_C = \pm v_C \frac{f_{1x}}{\sqrt{f_{1x}^2 + f_{1y}^2}} , \\ \dot{z}_C = 0 . \end{cases} \tag{2.78}$$

While solving the set of differential equations (2.78) the following initial conditions were assumed: $x_C\,(0) = 0.46$ [m], $y_C\,(0) = 0$ [m], and while solving differential equations (2.75) the assumed initial values of manipulator arms' rotation angles were $q_1\,(0) = 0$ [rad], $q_2\,(0) = 0.1653$ [rad], $q_3\,(0) = -0.1653$ [rad]. The adopted geometry of the Scorbot-ER 4pc RM corresponds to the parametric data included in Table 2.2.

The velocity values of the end-effector's point $C$ $v_C$, calculated from relation (2.77), are shown in Fig. 2.13a. The projection of the velocity vector on the axis tangent to the point's motion path takes either positive or negative values for individual motion periods. Each of the $m = 6$ periods consists of the acceleration phase, where $v_C$ changes from $v_C = 0$ [m/s] to $v_C = \pm v_C^*$ [m/s], the constant velocity phase, where $v_C = \pm v_C^* = \text{const.}$, and the braking phase, where the velocity of point $C$ tends to zero. The path of point $C$, calculated from differential equations (2.78), is shown in Fig. 2.13b. Point $C$ moves on a circular path with the assumed value of the velocity vector; with point $S$ being the initial position, marked with the triangle in Fig. 2.13b. Point $G$ is the point of reversal, where the end-effector's point $C$ comes to a halt, followed by the second phase, where point $C$ moves along the same path from point $G$ to point $S$. These two phases make a full motion cycle that is repeated three times within $t \in < 0, 40 >$ [s].

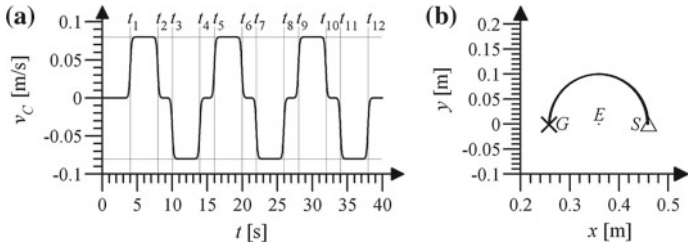



**Fig. 2.13** **a** Velocity profile of the end-effector's point $C$, **b** motion path of point $C$

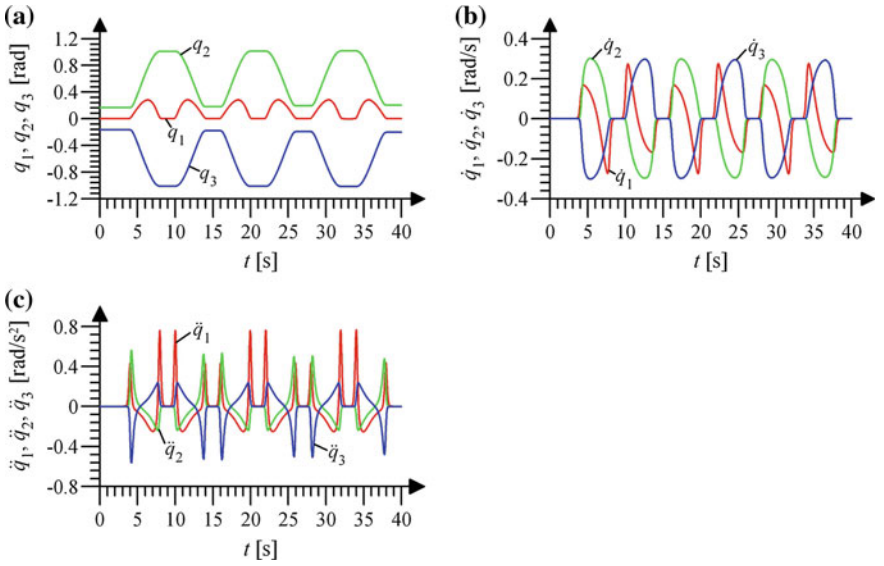



**Fig. 2.14** **a** Manipulator's links rotation angles $q_1, q_2, q_3$, **b** angular velocities $\dot{q}_1, \dot{q}_2, \dot{q}_3$, **c** angular accelerations $\ddot{q}_1, \ddot{q}_2, \ddot{q}_3$

The case described above illustrates a typical path planning/path execution problem that is challenged by industrial manipulators in the pick and place process.

Based on the assumed path and point $C$ velocity, the trajectory in the robot's configuration space was determined, by solving the inverse kinematics problem i.e. by calculating joints' variables from differential equations (2.75) such as: rotation angles $q_1$, $q_2$, $q_3$ (Fig. 2.14a), angular velocities $\dot{q}_1$, $\dot{q}_2$, $\dot{q}_3$ (Fig. 2.14b) and angular accelerations $\ddot{q}_1$, $\ddot{q}_2$, $\ddot{q}_3$ (Fig. 2.14c).

Thus obtained inverse kinematics problem solution, in the form of joints' variables, may constitute the desired reference trajectory to be tracked by the Scorbot-ER 4pc tracking control system.

### *2.2.2 Description of the Dynamics of a Robotic Manipulator*

Robotic manipulators are mechanical systems with a nonlinear dynamic description, which is due to the complexity of their structure. A dynamic model of such systems can be developed for example by adopting a classical mechanics approach or by means of the Lagrange's equations of the second kind. The basic issues relating to the modeling of robotic manipulator's dynamics are addressed in publications [2–4, 15, 18–20, 23].

The analysis of issues concerned with the dynamics of a RM consists in seeking correlations between the system's parameters of motion and the mechanisms that cause the motion. The forward dynamics problem is to determine the manipulator's kinematic parameters of motion resulting from the imposed forces, while the inverse dynamics problem is solved by determining the control variables required for the execution of the system's motion with regard to the assumed kinematic parameters.

The analysis of the RM's dynamics results in a mathematical model described with ordinary differential equations, with certain parameters and structure. The parameters of the model come in the form of coefficients in the differential equations of motion. However, it is difficult to determine their values, as they result from the geometry of the system, mass distribution or resistance to motion and thus can be defined in the process of parametric identification [3, 5, 12, 13, 18, 21–23]. Besides parametric identification the dynamic model may be used for the synthesis of the manipulator's tracking control systems. The model usually captures the most essential effects that occur in the manipulator's motion, due to the computational complexity and difficulty in measuring certain quantities. The dynamics of actuators is often deemed negligible and thus not considered, given the short time constants of the applied electric motors.

An important issue is the sensitivity of the mathematical model to changes in parameters [5, 21–23]. A sensitivity analysis allows to identify the impact of individual parameters on the accuracy of the mathematical model that can be simplified by isolating the parameters that have no significant influence on the model. The reduction of complexity allows the model to be applied in control based on the model performed in the real-time. A description of the Scorbot-ER 4pc dynamics model sensitivity analysis can be found in publications [22, 23].

This chapter presents a model of the dynamics of a three-degrees-of-freedom RM based on the Scorbot-ER 4pc robot. The model was derived using the Lagrange's equations of the second kind [22, 23]. The schematic diagram of the manipulator's kinematic chain is shown in Fig. 2.15.

The following denotations are used in Fig. 2.15: point $C$ – TCP, $|OO'| = d_1$, $|O'A| = l_1, |AB| = l_2, |BC| = l_3$ – dimensions resulting from the geometry of RM's kinematic chain, $u_1, u_2, u_3$ – links movement control signals. Point $O$ on the RM's

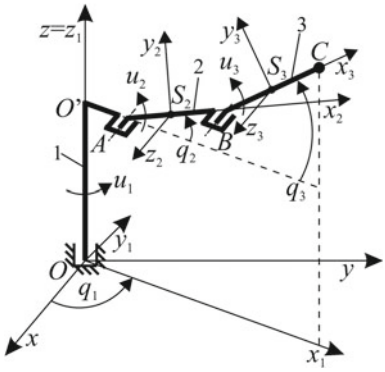



**Fig. 2.15** Schematic diagram of the Scorbot-ER 4pc robotic manipulator

base is bounded by the stationary Cartesian coordinate system $xyz$. Manipulator's link 1 is bounded by the moving coordinate system $x_1y_1z_1$ with origin at point $O$, where axis $z_1$ is identical to axis $z$ of the base system. Link 1 rotates about axis $z_1$ through an angle $q_1$. Links 2 and 3 rotate through angles $q_2$ and $q_3$, respectively, about joints' axes whose directions are perpendicular to the $x_1z_1$ plane and that pass through points $A$ and $B$. Link 3 rotation angle, $q_3$, is independent from link 2 rotation angle, $q_2$. Links' 2 and 3 resultant motion is composed of links' rotation motion with respect to joints and the transportation of link 2 imposed by link 1, as well as the transportation of link 3 imposed by links 1 and 2.

Given the assumptions set out in Sect. 2.2, a model of the RM's dynamics was derived by means of the Lagrange's equation of the second kind, thus

$$\frac{d}{dt}\left(\frac{\partial L}{\partial \dot{q}_j}\right) - \frac{\partial L}{\partial q_j} = Q_j \ , \tag{2.79}$$

$q_j$ – $j$th generalized coordinate, $Q_j$ – $j$th generalized force, $L$ – Lagrangian function is expressed by the relation

$$L = E - U \ , \tag{2.80}$$

where $E$ – kinetic energy of the system, $U$ – potential energy of the system. To formulate Lagrange's equations it is necessary to determine the kinetic and potential energy, and the generalized forces acting on the system. The kinetic energy of a multilink system is expressed by

$$E = \frac{1}{2}\dot{\mathbf{q}}^T \mathbf{M}(\mathbf{q})\,\dot{\mathbf{q}} \ , \tag{2.81}$$

where $\mathbf{M}(\mathbf{q})$ – inertia matrix, $\mathbf{M}(\mathbf{q}) \in \Re^{nxn}$. Since no deformations are considered, the manipulator's potential results only from the mass potentials of individual links of the kinematic chain within Earth's gravitational field, and is expressed by a function of generalized coordinates. Thus, the Lagrangian function is written as

$$L = \frac{1}{2}\dot{\mathbf{q}}^T \mathbf{M}(\mathbf{q})\,\dot{\mathbf{q}} - U(\mathbf{q}) \ . \tag{2.82}$$

By substituting relation (2.82) to Lagrange's equation (2.79) and performing model sensitivity analysis together with all the necessary computations given in [22, 23], the following equation of manipulator's dynamics was obtained

$$\mathbf{M}(\mathbf{q})\,\ddot{\mathbf{q}} + \mathbf{C}(\mathbf{q}, \dot{\mathbf{q}})\,\dot{\mathbf{q}} + \mathbf{F}(\dot{\mathbf{q}}) + \mathbf{G}(\mathbf{q}) + \boldsymbol{\tau}_d(t) = \mathbf{u} \ , \tag{2.83}$$

where $\mathbf{q}$ – vector of generalized coordinates, including manipulator's links rotation angles, $\mathbf{M}(\mathbf{q})$ – inertia matrix, $\mathbf{C}(\mathbf{q}, \dot{\mathbf{q}})\,\dot{\mathbf{q}}$ – vector of moments resulting from centrifugal and Coriolis forces, $\mathbf{F}(\dot{\mathbf{q}})$ – resistance to motion vector, $\mathbf{G}(\mathbf{q})$ – vector of

moments resulting from gravitational forces, $\boldsymbol{\tau}_d(t)$ – vector of bounded disturbance moments, $\mathbf{u}$ – control signals vector.

Matrices $\mathbf{M}(\mathbf{q})$, $\mathbf{C}(\mathbf{q}, \dot{\mathbf{q}})$, and vectors $\mathbf{F}(\dot{\mathbf{q}})$, $\mathbf{G}(\mathbf{q})$, $\boldsymbol{\tau}_d(t)$, $\mathbf{u}$, take the form

$$\begin{aligned}
\mathbf{M}(\mathbf{q}) &= \begin{bmatrix} M_{1,1} & 0 & 0 \\ 0 & p_6 & M_{2,3} \\ 0 & M_{3,2} & p_7 \end{bmatrix}, \\
\mathbf{C}(\mathbf{q}, \dot{\mathbf{q}}) &= \begin{bmatrix} -b\dot{q}_2 - c\dot{q}_3 & -b\dot{q}_1 & -c\dot{q}_1 \\ b\dot{q}_1 & 0 & C_{2,3} \\ c\dot{q}_1 & C_{3,2} & 0 \end{bmatrix}, \\
\mathbf{F}(\dot{\mathbf{q}}) &= \begin{bmatrix} p_8\dot{q}_1 + p_{11}\mathrm{sgn}(\dot{q}_1) \\ p_9\dot{q}_2 + p_{12}\mathrm{sgn}(\dot{q}_2) \\ p_{10}\dot{q}_3 + p_{13}\mathrm{sgn}(\dot{q}_3) \end{bmatrix}, \\
\mathbf{G}(\mathbf{q}) &= \begin{bmatrix} 0 \\ p_1 g\cos(q_2) \\ p_2 g\cos(q_3) \end{bmatrix}, \\
\boldsymbol{\tau}_d(t) &= \begin{bmatrix} \tau_{d1} \\ \tau_{d2} \\ \tau_{d3} \end{bmatrix}, \\
\mathbf{u}(t) &= \begin{bmatrix} u_1 \\ u_2 \\ u_3 \end{bmatrix},
\end{aligned} \tag{2.84}$$

where

$$\begin{aligned}
M_{1,1} &= 2p_1 l_1 \cos(q_2) + 2p_2 (l_1 + l_2\cos(q_2))\cos(q_3) + \tfrac{1}{2}p_3\cos(2q_2) + \\
&\quad + \tfrac{1}{2}p_4\cos(2q_3) + p_5, \\
M_{2,3} &= M_{3,2} = p_2 l_2 \cos(q_3 - q_2), \\
b &= p_1 l_1 \sin(q_2) + p_2 l_2 \sin(q_2)\cos(q_3) + \tfrac{1}{2}p_3\sin(2q_2), \\
c &= p_2 (l_1 + l_2\cos(q_2))\sin(q_3) + \tfrac{1}{2}p_4\sin(2q_3), \\
C_{2,3} &= -p_2 l_2 \sin(q_3 - q_2)\dot{q}_3, \\
C_{3,2} &= p_2 l_2 \sin(q_3 - q_2)\dot{q}_2,
\end{aligned} \tag{2.85}$$

where $\mathbf{p} = [p_1, \ldots, p_{13}]^T$ – vector of RM's parameters, which result from the geometry of the object, distribution of masses and resistance to motion, $g$ – gravitational acceleration, $g = 9.81\left[\frac{m}{s^2}\right]$.

The values of individual parameters are expressed by coefficients grouped as follows

$$
\begin{aligned}
p_1 &= m_2 l_{c2} + (m_3 + m_C)\, l_2 \ , \\
p_2 &= m_3 l_{c3} + m_C l_3 \ , \\
p_3 &= m_2 l_{c2}^2 + (m_3 + m_C)\, l_2^2 - I_{2xx} + I_{2yy} \ , \\
p_4 &= m_3 l_{c3}^2 + m_C l_3^2 - I_{3xx} + I_{3yy} \ , \\
p_5 &= I_{1yy} + \tfrac{1}{2}\left(I_{2xx} + I_{2yy} + I_{3xx} + I_{3yy}\right) + m_2\left(l_1^2 + \tfrac{1}{2} l_{c2}^2\right) + \\
&\quad + m_3\left(l_1^2 + \tfrac{1}{2} l_2^2 + \tfrac{1}{2} l_{c3}^2\right) + m_C\left(l_1^2 + \tfrac{1}{2} l_2^2 + \tfrac{1}{2} l_3^2\right) \ , \\
p_6 &= m_2\left(l_2^2 + l_{c2}^2\right) + m_C l_2^2 + I_{2zz} \ , \\
p_7 &= m_3 l_{c3}^2 + l_3^2 + I_{3zz} \ , \\
p_8 &= F_{v1} \ , \\
p_9 &= F_{v2} \ , \\
p_{10} &= F_{v3} \ , \\
p_{11} &= F_{C1} \ , \\
p_{12} &= F_{C2} \ , \\
p_{13} &= F_{C3} \ ,
\end{aligned}
\tag{2.86}
$$

where $m_i$ – manipulator's $i$th link mass, $m_C$ – gripper mass concentrated at TCP, $l_i$ – the $i$th link length, $l_{ci}$ – distance of the $i$th link's center of mass from the $i-1$ link's end, $I_{ixx}$, $I_{iyy}$, $I_{izz}$ – mass moments of inertia of the $i$th link with respect to $x_i$, $y_i$, $z_i$ axes, $F_{vi}$ – the $i$th link viscous friction coefficient, $F_{Ci}$ – moment of dry friction, $i = 1, 2, 3$. The construction of the resistance to motion vector $\mathbf{F}(\dot{\mathbf{q}})$ results from the assumed approximation of the resistance to motion moments of each kinematic pair with the application of moments that result from the viscous friction ($F_{vi}\dot{q}_i$) and the dry friction ($F_{Ci}\mathrm{sgn}(\dot{q}_i)$).

The set of Eq. (2.83) can be written in a linear form with respect to parameters $\mathbf{p}$

$$
\mathbf{Y}(\mathbf{q}, \dot{\mathbf{q}}, \ddot{\mathbf{q}})^T \mathbf{p} + \boldsymbol{\tau}_d(t) = \mathbf{u} \ , \tag{2.87}
$$

where $\mathbf{Y}(\mathbf{q}, \dot{\mathbf{q}}, \ddot{\mathbf{q}})$ – the so-called regression matrix, which takes the form

$$
\mathbf{Y}(\mathbf{q}, \dot{\mathbf{q}}, \ddot{\mathbf{q}}) = \left[\begin{array}{ccc|ccc|ccc|ccc}
Y_{11} & Y_{12} & Y_{13} & Y_{14} & \ddot{q}_1 & 0 & 0 & \dot{q}_1 & 0 & 0 & \mathrm{sgn}(\dot{q}_1) & 0 & 0 \\
\hline
Y_{21} & Y_{22} & Y_{23} & 0 & 0 & \ddot{q}_2 & 0 & 0 & \dot{q}_2 & 0 & 0 & \mathrm{sgn}(\dot{q}_2) & 0 \\
\hline
0 & Y_{32} & 0 & Y_{34} & 0 & 0 & \ddot{q}_3 & 0 & 0 & \dot{q}_3 & 0 & 0 & \mathrm{sgn}(\dot{q}_3)
\end{array}\right]^T \ , \tag{2.88}
$$

where

$$
\begin{aligned}
Y_{11} &= 2 l_1 \cos(q_2)\, \ddot{q}_1 - 2 l_1 \sin(q_2)\, \dot{q}_2 \dot{q}_1 \ , \\
Y_{12} &= 2\left(l_1 + l_2 \cos(q_2)\right)\left(\cos(q_3)\, \ddot{q}_1 - \sin(q_3)\, \dot{q}_3 \dot{q}_1\right) - 2 l_2 \sin(q_2) \cos(q_3)\, \dot{q}_2 \dot{q}_1 \ , \\
Y_{13} &= \tfrac{1}{2} \cos(2q_2)\, \ddot{q}_1 - \sin(2q_2)\, \dot{q}_2 \dot{q}_1 \ , \\
Y_{14} &= \tfrac{1}{2} \cos(2q_3)\, \ddot{q}_1 - \sin(2q_3)\, \dot{q}_3 \dot{q}_1 \ , \\
Y_{21} &= l_1 \sin(q_2)\, \dot{q}_1^2 + g \cos(q_2) \ , \\
Y_{22} &= l_2 \cos(q_3 - q_2)\, \ddot{q}_3 + l_2 \sin(q_2) \cos(q_3)\, \dot{q}_1^2 - l_2 \sin(q_3 - q_2)\, \dot{q}_3^2 \ , \\
Y_{23} &= \tfrac{1}{2} \sin(2q_2)\, \dot{q}_1^2 \ , \\
Y_{32} &= l_2 \cos(q_3 - q_2)\, \ddot{q}_2 + \left(l_1 + l_2 \cos(q_2)\right) \sin(q_3)\, \dot{q}_1^2 + l_2 \sin(q_3 - q_2)\, \dot{q}_2^2 + g \cos(q_3) \ , \\
Y_{34} &= \tfrac{1}{2} \sin(2q_3)\, \dot{q}_1^2 \ .
\end{aligned}
\tag{2.89}
$$

**Table 2.3** Asummed parametric values of the Scorbot-ER 4pc robotic manipulator

| Parameter | Value (no load) ($\mathbf{p}$) | Parameter | Value (load applied) ($\mathbf{p}_d$) | Unit |
|---|---|---|---|---|
| $p_1$ | 0.0065 | $p_{d1}$ | 0.0082 | kgm |
| $p_2$ | 0.0018 | $p_{d2}$ | 0.0041 | kgm |
| $p_3$ | 0.0113 | $p_{d3}$ | 0.0161 | kgm$^2$ |
| $p_4$ | 0.0064 | $p_{d4}$ | 0.0113 | kgm$^2$ |
| $p_5$ | 0.0114 | $p_{d5}$ | 0.0163 | kgm$^2$ |
| $p_6$ | 0.0113 | $p_{d6}$ | 0.0162 | kgm$^2$ |
| $p_7$ | 0.0065 | $p_{d7}$ | 0.0113 | kgm$^2$ |
| $p_8$ | 0.5276 | $p_{d8}$ | 0.5345 | Nms |
| $p_9$ | 0.5232 | $p_{d9}$ | 0.5340 | Nms |
| $p_{10}$ | 0.5235 | $p_{d10}$ | 0.5342 | Nms |
| $p_{11}$ | 0.0195 | $p_{d11}$ | 0.0221 | Nm |
| $p_{12}$ | 0.0182 | $p_{d12}$ | 0.0216 | Nm |
| $p_{13}$ | 0.0183 | $p_{d13}$ | 0.0217 | Nm |

A set of nominal parameters of the Scorbot-ER 4pc RM was assumed and denoted by $\mathbf{p}$, whereas the second set of parameters denoted by $\mathbf{p}_d$ relates to the manipulator with the gripper carrying a load of $m_L = 1$ [kg]. The parameters $\mathbf{p}_d$ were applied to simulate disturbance during the robot's movement. Both sets of parameters are presented in Table 2.3.

The inverse dynamics model of the RM can be defined based on Eq. (2.83), thus

$$\ddot{\mathbf{q}} = \mathbf{M}^{-1}(\mathbf{q}) \left[ \mathbf{u} - \mathbf{C}(\mathbf{q}, \dot{\mathbf{q}}) \dot{\mathbf{q}} - \mathbf{F}(\dot{\mathbf{q}}) - \mathbf{G}(\mathbf{q}) - \boldsymbol{\tau}_d(t) \right] . \tag{2.90}$$

Equation (2.90) is used further in this work for the modeling of the RM's motion by means of the generated control signals.

By applying Euler's method of approximation of continuous derivative by a difference, and substituting $\mathbf{z}_1 = \mathbf{q}$, $\mathbf{z}_2 = \dot{\mathbf{q}}$ to (2.90), in the same manner as in Sect. 2.1.2, the following discrete description of the RM's dynamics was obtained

$$\begin{aligned} \mathbf{z}_{1\{k+1\}} &= \mathbf{z}_{1\{k\}} + h\mathbf{z}_{2\{k\}} , \\ \mathbf{z}_{2\{k+1\}} &= \mathbf{z}_{2\{k\}} - h\mathbf{M}^{-1}(\mathbf{z}_{1\{k\}}) \left[ \mathbf{C}(\mathbf{z}_{1\{k\}}, \mathbf{z}_{2\{k\}}) \mathbf{z}_{2\{k\}} + \mathbf{F}(\mathbf{z}_{2\{k\}}) + \mathbf{G}(\mathbf{z}_{1\{k\}}) + \boldsymbol{\tau}_{d\{k\}} - \mathbf{u}_{\{k\}} \right] , \end{aligned} \tag{2.91}$$

where $\mathbf{z}_{1\{k\}} = \left[ z_{11\{k\}}, z_{12\{k\}}, z_{13\{k\}} \right]^T$ – vector of links' discrete angles of rotation corresponding to the continuous vector $\mathbf{q}$, $\mathbf{z}_{2\{k\}} = \left[ z_{21\{k\}}, z_{22\{k\}}, z_{23\{k\}} \right]^T$ – vector of discrete angular velocities that corresponds to the continuous vector $\dot{\mathbf{q}}$, $k$ – index of iteration steps, $h$ – time discretization parameter. Difference equations of RM's dynamics (2.91) that were derived by means of Lagrange's equations of the second kind are used further in this work for the modeling of motion of a controlled object,

while a discrete form of relation (2.83) was applied in the synthesis of manipulator's TCP tracking control algorithms.

The structural properties of the RM's dynamic model (2.83) are used in the synthesis of tracking control algorithms. These properties are presented below.

**Structural Properties of the RM's Mathematical Model**

Description of the RM's dynamics in the form of Eq. (2.83) complies with the following assumptions [4, 18, 19]:

1. Inertia matrix $\mathbf{M}(\mathbf{q})$ is symmetric and positive-definite, and meets the conditions
$$\sigma_{\min}(\mathbf{M}(\mathbf{q}))\,\mathbf{I} \leq \mathbf{M}(\mathbf{q}) \leq \sigma_{\max}(\mathbf{M}(\mathbf{q}))\,\mathbf{I}\,, \tag{2.92}$$
where $\mathbf{I}$ – identity matrix, $\sigma_{\min}(\mathbf{M}(\mathbf{q}))$, $\sigma_{\max}(\mathbf{M}(\mathbf{q}))$ – respectively, minimum and maximum strictly positive eigenvalue of the interia matrix.
2. Matrix $\mathbf{C}(\mathbf{q}, \dot{\mathbf{q}})$ is such that the matrix
$$\mathbf{S}(\mathbf{q}, \dot{\mathbf{q}}) = \dot{\mathbf{M}} - 2\mathbf{C}(\mathbf{q}, \dot{\mathbf{q}})\,, \tag{2.93}$$
is skew-symmetric. Thus, the following relation holds
$$\boldsymbol{\xi}^T \mathbf{S}(\mathbf{q}, \dot{\mathbf{q}})\,\boldsymbol{\xi} = \mathbf{0}\,, \tag{2.94}$$
where $\boldsymbol{\xi}$ – any given vector of appropriate dimension.
3. Vector of disturbances $\boldsymbol{\tau}_d(t)$ acting on the RM is bounded so that $\|\tau_{dj}(t)\| \leq b_{dj}$, where $b_{dj}$ is a positive constant, $j = 1, 2, 3$.
4. The RM's dynamic Eq. (2.83) can be written in a linear form with respect to the parameters, hence
$$\mathbf{M}(\mathbf{q})\,\ddot{\mathbf{q}} + \mathbf{C}(\mathbf{q}, \dot{\mathbf{q}})\,\dot{\mathbf{q}} + \mathbf{F}(\dot{\mathbf{q}}) + \mathbf{G}(\mathbf{q}) + \boldsymbol{\tau}_d(t) = \mathbf{Y}(\mathbf{q}, \dot{\mathbf{q}}, \ddot{\mathbf{q}})^T\,\mathbf{p} + \boldsymbol{\tau}_d(t) = \mathbf{u}\,, \tag{2.95}$$
vector of parameters $\mathbf{p}$ shall consist of a minimum number of linearly independent elements.
5. The following relation holds for any two $\mathbf{x}$ and $\mathbf{y}$ vectors
$$\mathbf{C}(\mathbf{q}, \mathbf{x})\,\mathbf{y} = \mathbf{C}(\mathbf{q}, \mathbf{y})\,\mathbf{x}\,. \tag{2.96}$$
6. Matrix $\mathbf{C}(\mathbf{q}, \dot{\mathbf{q}})$ meets the condition
$$\|\mathbf{C}(\mathbf{q}, \dot{\mathbf{q}})\| \leq K_C \|\dot{\mathbf{q}}\|\,, \tag{2.97}$$
where $K_C > 0$.

7. Vector $\mathbf{C}(\mathbf{q}, \dot{\mathbf{q}})\,\dot{\mathbf{q}}$ meets the condition

$$\|\mathbf{C}(\mathbf{q}, \dot{\mathbf{q}})\,\dot{\mathbf{q}}\| \leq k_C \|\dot{\mathbf{q}}\|^2 , \tag{2.98}$$

where $k_C > 0$.
8. Vector $\mathbf{F}(\dot{\mathbf{q}})$ meets the condition

$$\|\mathbf{F}(\dot{\mathbf{q}})\| \leq K_F \|\dot{\mathbf{q}}\| + k_F , \tag{2.99}$$

where $K_F > 0$, and $k_F > 0$.
9. Vector $\mathbf{G}(\mathbf{q})$ meets the condition

$$\|\mathbf{G}(\mathbf{q})\| \leq k_G , \tag{2.100}$$

where $k_G > 0$.

#### 2.2.2.1 Simulation of Inverse Dynamics Problem of a Robotic Manipulator

In the simulation of the manipulator's motion the robot's TCP moves along the desired circular segment path with center $E$ and radius $R = 0.1$ [m]. The inverse kinematics solution trajectory from Sect. 2.2.1.2 was used. The values of control signals $u_1$, $u_2$ and $u_3$ were generated based on manipulator's parameters of motion such as rotation angles ($\mathbf{q}$), angular velocities ($\dot{\mathbf{q}}$) and angular accelerations ($\ddot{\mathbf{q}}$), according to relation (2.83). The control signals cause the robotic manipulator's TCP motion on the determined path. The joint variables take their set values. The nominal values of manipulator's parameters $\mathbf{p}$ were assumed as defined in Table 2.3. The diagram of the defined TCP's motion path is shown in Fig. 2.16a, pre-determined rotation angles of manipulator's links $(q_1, q_2, q_3)$ and angular velocities values $(\dot{q}_1, \dot{q}_2, \dot{q}_3)$ are illustrated in Fig. 2.16b,c, respectively. Figure 2.16d presents the generated control signals $u_1$, $u_2$ and $u_3$.

The desired reference trajectory consists of several motion phases, which result from the TCP's defined motion path in a pick and place type of task, where point $S$ marks the TCP's initial position and point $G$ is the path's reversal point. The trajectory is executed such that the TCP's motion cycle (from point $S$ to point $G$ and back) is performed three times. Each time the manipulator's TCP stops at point $S$ and $G$ for the period $t = 2$ [s]. In the initial phase of the simulation ($t \in < 0, 4 >$), the signals controlling links 2 and 3 movement take non-zero values, though no manipulator movement occurs. This is because the model of dynamics (2.83) includes the vector of moments resulting from gravitational forces $\mathbf{G}(\mathbf{q})$ that must be balanced by control signals to ensure the performance of motion parameters. In the case of link 1, whose

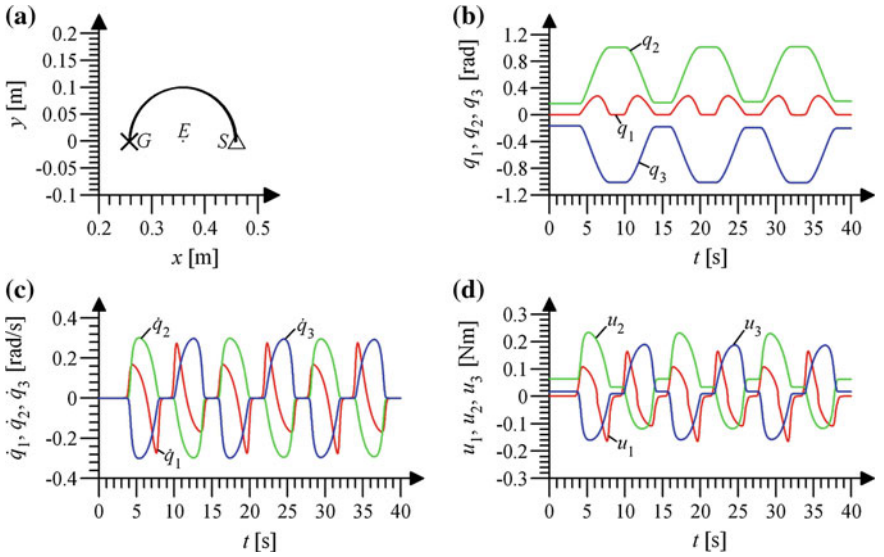



**Fig. 2.16** **a** Desired motion path of point $C$ attached to the manipulator's arm, **b** links rotation angles $q_1, q_2, q_3$, **c** angular velocities $\dot{q}_1, \dot{q}_2, \dot{q}_3$, **d** control signals $u_1, u_2, u_3$

axis of rotation is parallel to $z$-axis of the global coordinate system, there is no impact of the moments of gravitational forces upon the link movement. In the following motion phases, the values of control signals depend on the parameters of motion $\mathbf{q}$, $\dot{\mathbf{q}}$ and $\ddot{\mathbf{q}}$, where the dominant influence is exercised by the vector of moments resulting from the resistance to motion $\mathbf{F}(\dot{\mathbf{q}})$, whose values are the functions of links' angular velocities vector $\dot{\mathbf{q}}$.

## References

1. Active Media Robotics Pioneer 2/PeopleBot Operations Manual, Active Media, version 9, Peterborough (2001)
2. Angeles, J.: Fundamentals of Robotic Mechanical Systems: Theory, Methods, and Algorithms. Springer, New York (2007)
3. Canudas de Wit, C., Siciliano, B., Bastin, G.: Theory of Robot Control. Springer, London (1996)
4. Craig, J.J.: Introduction to Robotics. Prentice Hall, Upper Saddle River (2005)
5. Eykhoff, P.: Identification in Dynamical Systems. (in Polish) PWN, Warsaw (1980)
6. Fierro, R., Lewis F.L.: Control of a nonholonomic mobile robot using neural networks. IEEE Trans. Neural Netw. **9**(4), 589–600 (1998)
7. Giergiel, J., Hendzel, Z., Zylski, W.: Modeling and Control of Wheeled Mobile Robots. (in Polish) Scientific Publishing PWN, Warsaw (2002)
8. Giergiel, J., Zylski, W.: Description of motion of a mobile robot by Maggie's equations. JTAM **43**, 511–521 (2005)

9. Gierlak, P.: Analysis of the kinematics of the 5DOF manipulator. (in Polish) Scientific Letters of Rzeszow University of Technology, Mechanics **86**, 491–500 (2014)
10. Gutowski, R.: Analytical Mechanics. (in Polish) PWN, Warsaw (1971)
11. Hendzel, Z.: Tracking Control of Wheeled Mobile Robots. (in Polish) Rzeszow University of Technology Publishing House, Rzeszow (1996)
12. Hendzel, Z., Nawrocki, M.: Neural identification for Scorbot manipulator. (in Polish) Modelling. Eng. **36**, 135–142 (2008)
13. Hendzel, Z., Nawrocki, M.: Identification of the robot model parameters. (in Polish) Acta Mech. Autom. **4**, 69–73 (2010)
14. Hendzel, Z., Trojnacki, M.: Neural Network Control of Mobile Wheeled Robots. (in Polish) Rzeszow University of Technology Publishing House, Rzeszow (2008)
15. Kozowski, K., Dutkiewicz, P., Wrblewski, W.: Modeling and Control of Robots. (in Polish) Scientific Publishing PWN, Warsaw (2003)
16. Morecki, A., Knapczyk, J.: Basis of Robotics: Theory and Elements of Manipulators and Robots. WNT, Warsaw (1999)
17. SCORBOT-ER 4pc User's Manual, Eshed Robotec, version A, Rosh Haayin (1999)
18. Slotine, J.J., Li, W.: Applied Nonlinear Control. Prentice Hall, New Jersey (1991)
19. Spong, M.W., Vidyasagar, M.: Robot Dynamics and Control. (in Polish) WNT, Warsaw (1997)
20. Tcho, K., Mazur, A., Dulba, I., Hossa R., Muszyski, R.: Mobile Manipulators and Robots. (in Polish) Academic Publ. Company PLJ, Warsaw (2000)
21. Zylski, W.: Kinematics and Dynamics of Wheeled Mobile Robotos. (in Polish) Rzeszow University of Technology Publishing House, Rzeszow (1996)
22. Zylski, W., Gierlak, P.: Modelling of Movement of Selected Manipulator. (in Polish) Acta Mech. Autom. **4**, 112–119 (2010)
23. Zylski, W., Gierlak, P.: Tracking Control of Robotic Manipulator. (in Polish) Rzeszow University of Technology Publishing House, Rzeszow (2014)



http://www.springer.com/978-3-319-68824-4

Intelligent Optimal Adaptive Control for Mechatronic Systems

Szuster, M.; Hendzel, Z.

2018, XI, 382 p. 224 illus., 119 illus. in color., Hardcover
ISBN: 978-3-319-68824-4